The Astrophysical Journal, 613:752–769, 2004 October 1
© 2004. The American Astronomical Society. All rights reserved. Printed in U.S.A.

A SAMPLE OF LOW-REDSHIFT BL LACERTAE OBJECTS. I. THE RADIO DATA

M. Giroletti and G. Giovannini
Istituto di Radioastronomia, via Gobetti 101, 40129 Bologna, Italy; and
Dipartimento di Astronomia, Università di Bologna, via Ranzani 1, 40127 Bologna, Italy

G. B. Taylor
National Radio Astronomy Observatory, P.O. Box O, Socorro, NM 87801

and

R. Falomo
Osservatorio Astronomico di Padova, vicolo Osservatorio 5, Padua, Italy
Received 2004 January 19; accepted 2004 June 9

ABSTRACT

We present a new sample of 30 nearby ($z < 0.2$) BL Lac objects, selected to study the nuclear as well as the large-scale properties of low-power radio sources. In this first paper, we show and discuss new radio data taken with the Very Large Array (19 objects at 1.4 GHz, either in A or C configuration, or both) as well as with the Very Long Baseline Array (15 sources at 5 GHz). On the kiloparsec scale, all objects exhibit a compact core and a variety of radio morphologies (jets, halos, and secondary compact components). On the parsec scale, we find weak cores and a few short, one-sided jets. From the jet/counterjet ratio, core dominance, and synchrotron self-Compton model, we estimate the intrinsic orientation and velocity of the jets. The resulting properties of BL Lac objects are similar to those of a parent population composed of FR I radio galaxies.

Subject headings: BL Lacertae objects: general — galaxies: active — galaxies: jets — galaxies: nuclei — radio continuum: galaxies

1. INTRODUCTION

Ever since the first suggestion of a possible unification of radio sources (e.g., Orr & Browne 1982), the viability for a comprehensive view of active galactic nuclei (AGNs) has been actively debated. A major achievement is the formulation of a scheme in which BL Lac objects and quasars are the aligned counterparts of edge-darkened (FR I) and edge-brightened (FR II) radio galaxies, respectively (e.g., Urry & Padovani 1995). However, many important issues still need to be worked out. In particular, the class of BL Lac objects and its unification to FR I radio galaxies is an incessant source of puzzling questions.

For many years, when only a few objects were known, an apparent dichotomy was present within the BL Lac population. This dichotomy was based initially on selection criteria, separating X-ray– and radio-selected objects. Later on, the dichotomy was refined according to the position of the low-energy peak in the spectral energy distribution (SED), with BL Lac objects classified as either low (LBL) or high (HBL) frequency peaked objects. LBLs have the peaks of emitted energy (νF_ν) in the infrared/optical and MeV/GeV bands, while HBLs peak at higher frequencies, namely, UV/X-ray and GeV/TeV; furthermore, other observational differences between LBLs and HBLs have been found, including the fact that HBLs have less dominant radio cores, a lower degree of optical polarization, and a possibly different cosmological evolution (see Rector et al. 2003 and references therein). However, multiwavelength studies of larger samples seem to have solved this dichotomy, showing that the SED of BL Lac objects (and emission-line blazars) form a continuum, and that the emission peaks shift to higher frequency as the bolometric luminosity decreases (the so-called *blazar sequence*; see Fossati et al. 1998). Donato et al. (2001) confirmed this trend considering more sources and hard X-ray data. Among possible explanations, Ghisellini et al. (1998) proposed that an increase in luminosity causes the emitting particles to suffer more severe radiative losses; in turn, this explains the shift of the peaks to lower frequency. There are, however, some problems with this scenario: following the discovery of a significant number of flat-spectrum radio quasars with flat $\alpha_{\rm RX}$ in a deep survey (the Deep X-Ray Radio Blazar Survey; see Perlman et al. 1998; Landt et al. 2001), Padovani et al. (2003) considered a large sample of $\sim$500 blazars, finding no evidence of anticorrelations between $\nu_{\rm peak}$ and radio power (or other related quantities), as expected from the blazar sequence. Moreover, Caccianiga & Marchã (2004) present a few examples of low radio power BL Lac objects with steep $\alpha_{\rm RX}$, suggesting that there may exist sources with a peak at low frequency and steep $\alpha_{\rm RX}$, as well as objects peaking at high frequency but still displaying flat $\alpha_{\rm RX}$ (see also Anton et al. 2004).

In spite of our advances in understanding, most physical parameters remain difficult to determine in BL Lac objects. Several papers (see, e.g., Falomo et al. 2002 and references therein) have addressed the long-debated issue of determining the mass of the central black hole, finding values of order 10^8–$10^9\ M_\odot$. The situation remains more complicated for the jet physics and main parameters. On one hand, we have constraints from the detection of very energetic GeV and TeV photons, which require Doppler factor values $\delta > 10$ (Tavecchio et al. 1998); on the other hand, lower values are preferred from radio observations and from the lack of measured superluminal motions in most TeV sources (Giroletti et al. 2004; Piner & Edwards 2004; Tingay & Edwards 2002). Even in sources where proper motions have been found (Homan et al. 2001; Jorstad et al. 2001), the estimated jet velocity from radio data is lower than the jet velocity required by high-energy photons. This discrepancy suggests that the γ-rays and the radio photons

may be produced in different regions of the jet, moving at different bulk velocities or differently oriented with respect to the line of sight. Furthermore, it is also possible that the jet has a dual *transverse* velocity or energetic structure; this may be needed to explain the different behavior of optical cores in BL Lac objects with respect to FR I radio galaxies (Chiaberge et al. 2000). In particular, the optical radiation could come from a faster spine, while the radio emission could originate in a slower, external layer of the jet. Evidence for a velocity structure in parsec-scale jets has been found in some sources such as 1144+35, Mrk 501, 3C 264, M87, 0331+39, and 1055+018 (see, e.g., Sol et al. 1989; Hanasz & Sol 1996; Giovannini et al. 2001; Giroletti et al. 2004; Perlman et al. 1999, 2001; Attridge et al. 1999). The presence of a velocity structure could be due to the jet interaction with the interstellar medium (ISM) (Giovannini et al. 2001) or could be an intrinsic jet property (Meier 2003).

As a matter of fact, the radio interferometry technique is an unique tool for determining parameters of the jet in the region from a few parsecs out to the kiloparsec-scale structure, by means of studying observational properties such as jet sidedness, core dominance, and proper motion of knots (Giovannini 2003). Very long baseline interferometry (VLBI) studies have yielded significant results for a number of sources, including a possible signature of the double-velocity structure in the limb-brightened jet of Mrk 501 (Giroletti et al. 2004). However, systematic and detailed VLBI studies on sizeable samples of BL Lac objects are mostly based on bright, flux-limited catalogs, such as the 1 Jy sample (Stickel et al. 1991). By its very definition, this sample consists mostly of powerful and distant objects. These bright sources have yielded some interesting results, among which is a high incidence of FR II structures in the parent population (Rector & Stocke 2001; Cassaro et al. 1999). Moreover, objects in this sample often present a significant bending between parsec- and kiloparsec-scale structure (Cassaro et al. 2002), resulting in a peculiar bimodal distribution of the misalignment angle between the structure on the two scales (see also Appl et al. 1996 and references therein).

As for the weaker objects, parsec-scale studies similar to those discussed above are still missing or based on small numbers of objects (Rector et al. 2003; Kollgaard et al. 1996). Given the SED shape for BL Lac objects, objects weak in the radio are usually classified as HBLs. Thus far, almost all BL Lac objects detected at TeV energies belong to this subclass. Moreover, weak objects are more easily found at low redshift, so that the high angular resolution of VLBI techniques allows observers to investigate the very innermost regions (1 mas $\sim$ 2 pc at $z = 0.1$).[1]

In order to investigate the above issues and to extend the current view to the low-z objects, we concentrated our attention on the sample of Falomo et al. (2000), who studied the host galaxies of 30 low-redshift ($z < 0.2$) BL Lac objects with the *Hubble Space Telescope* (*HST*). We carried out new radio observations of this sample to look for differences in morphology with more powerful objects and to derive parameters for jet physics. In this paper, we present the new observations and summarize data from the literature. By using all available data, we can study the intrinsic power and parent population. In a forthcoming paper (M. Giroletti et al. 2004, in preparation), we will focus on the radio/optical comparison.

[1] Throughout this paper, we assume $H_0 = 71$ km s^{-1} Mpc^{-1} and $q_0 = 0.5$.

The sample selection is illustrated in § 2, along with the main results of Falomo et al. (2000). Our observations are described in § 3; we present the results in § 4 and discuss them in § 5. Finally, § 6 summarizes the main results.

2. THE SAMPLE

2.1. *Sample Selection*

By merging seven flux-limited samples,[2] Scarpa et al. (2000) have collected a total of 132 BL Lac objects. The *HST* snapshot image survey of BL Lac objects (Urry et al. 2000; Scarpa et al. 2000) has provided a homogeneous set of short-exposure, high-resolution images through the F702W filter for 110 objects in the sample. From this large data set, Falomo et al. (2000) extracted a subsample of 30 low-redshift ($z < 0.2$) objects for which it was possible to perform a detailed study of the properties of the host galaxy.

We now discard three objects from this sample: 1853+671 and 2326+174, which have a redshift slightly larger than 0.2 ($z = 0.212$ and 0.213, respectively), and 2005−489, which is too far south to be observed with comparable quality high-resolution imaging. Conversely, we add three more objects, which also have $z < 0.2$ and high-quality *HST* observations available. The objects are 1215+303 ($z = 0.130$; E. S. Perlman et al. 2004, private communication), 2254+074 ($z = 0.190$), and 1652+398 (Mrk 501; $z = 0.034$). In total we have 30 objects. Although the sample cannot be considered complete, the selection process appears free from significant biases with respect to source orientation and jet velocity.

Table 1 presents the full list of objects in the sample.[3] HBLs are clearly dominant, and most objects have been originally selected at X-ray energies. This selection is significantly different from most previous studies at radio frequencies. We note that HBLs have lower total luminosities and are particularly weak in the radio. Figure 1 plots, as histograms, the distribution of total power at 1.4 GHz for objects in the present sample compared to the 1 Jy sample. The two distributions are significantly different, with $\langle \log P_{1.4\,\mathrm{GHz}} \rangle = 24.7 \pm 0.6$ and 26.7 ± 0.9 W Hz^{-1}, respectively (some objects in the 1 Jy sample lack redshift information and were not considered). This is largely due to the large flux limit of the 1 Jy sample; furthermore, with no cut in redshift, it contains a number of high-z BL Lac objects that bias the sample toward more powerful objects.

However, we note that there is some overlap between the two populations. Six of the objects belong to both samples (1418+546, 1514−241, 1652+398, 1807+698, 2200+420, and 2254+074); indeed, these are well-known objects, such as BL Lac itself, Mrk 501, and 3C 371. In contrast, most of the weakest HBLs lack radio images on the parsec and/or kiloparsec scales.

2.2. *Host Galaxies: A Summary*

For these low-z objects it was possible with *HST* to investigate features and structures in the host galaxy that are

[2] The seven samples are 1 Jy (Stickel et al. 1991); S4 (Stickel & Kuehr 1994); PG (Green et al. 1986); HEAO-A2 (Piccinotti et al. 1982); HEAO-A3 (R. Remillard et al. 1999, unpublished); EMSS (Morris et al. 1991; Stocke et al. 1991; Rector et al. 2000); and Slew (Schachter et al. 1993; Perlman et al. 1996).

[3] The optical spectra of 0521−365 (Scarpa et al. 1995) and 2201+044 (Veron-Cetty & Veron 1993; Falomo et al. 1994) show emission and absorption lines and are similar to Seyfert 1 spectra but with lines of lower luminosity. At *HST* resolution the optical sources are fully resolved into nucleus, host galaxy, and a jet that contains some structures.

TABLE 1
OBJECTS IN THE SAMPLE

Number (1)	Name (IAU) (2)	Other Name (3)	z (4)	R.A. (5)	Decl. (6)	Class (7)	Sample (8)
1	0145+138	...	0.125	01 48 29.7	+14 02 18	H	Slew
2	0229+200	...	0.140	02 32 48.4	+20 17 16	H	HEAO-A3
3	0347−121	...	0.188	03 49 23.2	−11 59 27	H	HEAO-A3
4	0350−371	...	0.165	03 51 53.8	−37 03 46	H	EMSS
5	0521−365	...	0.055	05 22 58.0	−36 27 31	L	HEAO-A3
6	0548−322	...	0.069	05 50 40.8	−32 16 18	H	HEAO-A2
7	0706+591	...	0.125	07 10 30.0	+59 08 20	H	HEAO-A3
8	0806+524	...	0.137	08 09 49.1	+52 18 59	H	Slew
9	0829+046	...	0.180	08 31 48.9	+04 29 39	L	HEAO-A3
10	0927+500	...	0.188	09 30 37.6	+49 50 26	H	Slew
11	1101+384	Mrk 421	0.031	11 04 27.3	+38 12 32	H	HEAO-A3
12	1133+704	Mrk 180	0.046	11 36 26.4	+70 09 27	H	HEAO-A3
13	1212+078	...	0.136	12 15 10.9	+07 32 04	H	Slew
14	1215+303	...	0.130	12 17 52.1	+30 07 01	H	Slew
15	1218+304	...	0.182	12 21 21.9	+30 10 37	H	HEAO-A2
16	1229+643	...	0.164	12 31 31.4	+64 14 18	H	EMSS
17	1255+244	...	0.141	12 57 31.9	+24 12 40	H	Slew
18	1418+546	OQ 530	0.152	14 19 46.6	+54 23 15	L	PG
19	1426+428	...	0.129	14 28 32.6	+42 40 21	H	HEAO-A3
20	1440+122	...	0.162	14 42 48.2	+12 00 40	H	Slew
21	1514−241	AP Lib	0.049	15 17 41.8	−24 22 19	H	1 Jy
22	1652+398	Mrk 501	0.034	16 53 52.2	+39 45 37	H	1 Jy
23	1728+502	I Zw 187	0.055	17 28 18.6	+50 13 10	H	HEAO-A3
24	1807+698	3C 371	0.051	18 06 50.6	+69 49 28	L	1 Jy
25	1959+650	...	0.048	19 59 59.8	+65 08 55	H	HEAO-A3
26	2200+420	BL Lac	0.070	22 02 43.3	+42 16 40	L	1 Jy
27	2201+044	...	0.027	22 04 17.6	+04 40 02	L	HEAO-A3
28	2254+074	...	0.190	22 57 17.3	+07 43 12	L	1 Jy
29	2344+514	...	0.044	23 47 04.8	+51 42 18	H	Slew
30	2356−309	...	0.165	23 59 07.8	−30 37 40	H	HEAO-A3

NOTES.—Units of right ascension are hours, minutes, and seconds, and units of declination are degrees, arcminutes, and arcseconds. Col. (7): H, High-frequency peaked BL Lac object; L, Low-frequency peaked BL Lac object. Col. (8): 1 Jy (Stickel et al. 1991); HEAO-A2 (Piccinotti et al. 1982); HEAO-A3 (R. Remillard et al. 1999, unpublished); EMSS (Morris et al. 1991); Slew (Schachter et al. 1993; Perlman et al. 1996).

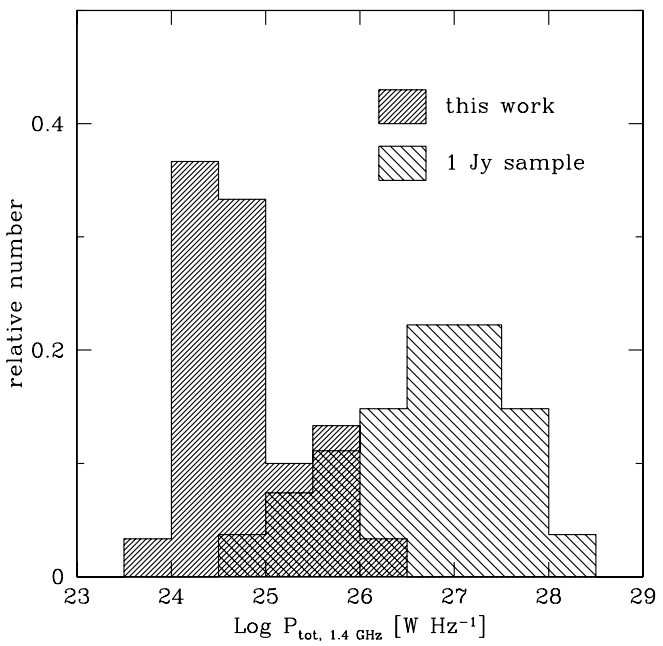

FIG. 1.—Histogram of total power distribution at 1.4 GHz for objects in our sample and in the 1 Jy sample. Data are from the NVSS survey (Condon et al. 1998) for our sample and from Rector & Stocke (2001) for the 1 Jy sample.

undetectable with ground-based observations (Falomo et al. 2000). The host galaxy can be investigated within less than 1 kpc from the nucleus (corresponding to $0\farcs3$ at $z = 0.2$). In particular, one can search for slight offsets of the nucleus with respect to the galaxy center, determine the presence of subcomponents in the host galaxy, investigate the detailed shape of the isophotes, and search for dust features and close companions.

The detailed analysis of *HST* images indicates that, in spite of the presence of the active nucleus, the host galaxy appears in most cases to be a completely "normal" elliptical galaxy. Both the ellipticity and the isophotal shape distributions are similar to those for radio galaxies and radio-quiet elliptical galaxies. This suggests that tidal interactions are very infrequent or are short-lived with respect to the nuclear activity timescale.

There are no indications of displacements and/or off-centering of the galaxy isophotes with respect to the nucleus, meaning that the unresolved nuclear source truly sits in the center of the galaxy. This rules out the microlensing hypothesis for BL Lac objects, which predicts frequent offsets for the nucleus with respect to the host galaxy.

The *HST* images have consistently shown that BL Lac hosts are virtually all massive elliptical galaxies (average luminosity $M_R = -23.7 \pm 0.6$ and effective radius $R_e = 10$ kpc) typically located in poor groups. Moreover, these data have shown that

TABLE 2
SUMMARY OF 1.4 GHz VLA OBSERVATIONS

Date	Configuration	Hours	Targets
2002 Feb 22	A	5	0706+591, 0806+524, 0829+046, 0927+500, 1133+704, 1212+078, 1218+304, 1229+643, 1255+244, 1426+428, 1728+502, 1959+650
2002 May 3	A	2.5	0145+138, 0229+200, 0347−121, 0350−371, 2254+074, 2344+514, 2356−309
2002 Oct 8	C	4.5	0145+138, 0229+200, 0347−121, 1728+502, 1807+698, 1959+650, 2254+074, 2344+514, 2356−309

no significant difference is present between the hosts of HBLs and those of LBLs in spite of the remarkable differences in their SEDs (Urry et al. 2000).

3. OBSERVATIONS AND DATA REDUCTION

Observations were aimed at completing the imaging for all the sources in the sample, both on arcsecond (Table 2) and milliarcsecond (Table 3) scales. We present the final images in Figures 2–6 (see Table 4 for image parameters). Objects with good images available in the literature were not reobserved; see Table 5 for a summary of references.

3.1. *Very Large Array Observations*

We obtained observations with the NRAO Very Large Array (VLA)[4] at 1.4 GHz on 2002 February 22 and May 3 in A configuration and on 2002 October 8 in C configuration (see Table 2 for a summary of the observations). In order to optimize the (u, v) coverage, we observed in snapshot mode with two or three scans per source at different hour angles. On average, each source was observed for about 16 minutes after allowing for observations of calibrators and slewing of the telescope. We used the NRAO Astronomical Image Processing System (AIPS) to reduce the data and perform imaging with the standard phase self-calibration technique. Amplitude self-calibration was used only for the strongest sources (>100 mJy) to obtain a better dynamic range. For fainter sources, amplitude self-calibration is not necessary since images are noise-limited and not dynamic range–limited; moreover, spurious solutions could be introduced because of the low signal-to-noise ratio. We produced images with different weight distribution (uniform and natural) and did not find significant differences. Images presented here have been obtained with a weight between the natural and uniform (ROBUST 0 in the task IMAGR in AIPS). This weighting scheme yields a typical final restoring beam of $\sim 1\farcs9 \times 1\farcs2$ for A configuration and of $\sim 15'' \times 11''$ for C configuration data; the average noise is $\sim$70 and $\sim$140 μJy beam^{-1}, respectively. Images of sources in the southern hemisphere have more elliptical beams and slightly higher noise.

In total, we imaged 19 objects with the array in A configuration and nine in C configuration. For the eight sources observed with both arrays, we combined the two final self-calibrated data set using the AIPS task DBCON. This yields better sensitivity (about a factor of $\sqrt{2}$) and intermediate resolution. However, the (u, v) coverage is not optimal, and the process of self-calibration can fail to converge, especially when extended flux detected in C configuration is overresolved by the A array. For this reason, we only present combined array images for five sources (0145+138, 0229+200, 0347−121, 1959+650, and 2356−309).

3.2. *Very Long Baseline Array Observations*

VLBI observations have been performed with the NRAO Very Long Baseline Array (VLBA) for 15 sources on 2002 February 17, 18, and 19, at a frequency of 5 GHz (see Table 3 for a summary of the observations). A single VLA antenna was substituted for the VLBA antenna at Pie Town. We recorded four intermediate frequencies (at 4971.49, 4979.49, 4987.49, and 4995.49 MHz) with 8 MHz bandwidth each, in full polarizations. The data were correlated in Socorro, and the reduction was performed in AIPS. All data were globally fringe-fitted (Schwab & Cotton 1983) and then self-calibrated. However, the VLA observations in A configuration provided us with new and precise position measurements. Since we had good positions for our target sources, we were able to avoid fringe-fitting the data for weak sources, which easily fails. Amplitude calibration was initially done using the standard method of measuring system temperatures and antenna gains calibration, followed by gain refinement using strong pointlike calibrators.

On average, we have 45 minutes of useful data for each source, providing a nominal thermal noise of $\sim$0.11 mJy beam^{-1}. All our images have noise figures within a factor of 2 from this. All sources are detected above the 3 σ level, even the weakest. For six sources, only a faint pointlike component was detected. For the remaining nine strongest sources, we

[4] The VLA is operated by the National Radio Astronomy Observatory, which is a facility of the National Science Foundation, operated under cooperative agreement by Associated Universities, Inc.

TABLE 3
SUMMARY OF 5 GHz VLBA OBSERVATIONS

Date	Hours	Targets
2002 Feb 17	6	0145+138, 0229+200, 0347−121, 0350−371, 2344+514, 2356−309
2002 Feb 18	4	0521−365, 0548−322, 0706+591, 0806+524
2002 Feb 19	5	1212+078, 1218+304, 1229+643, 1255+244, 1440+122

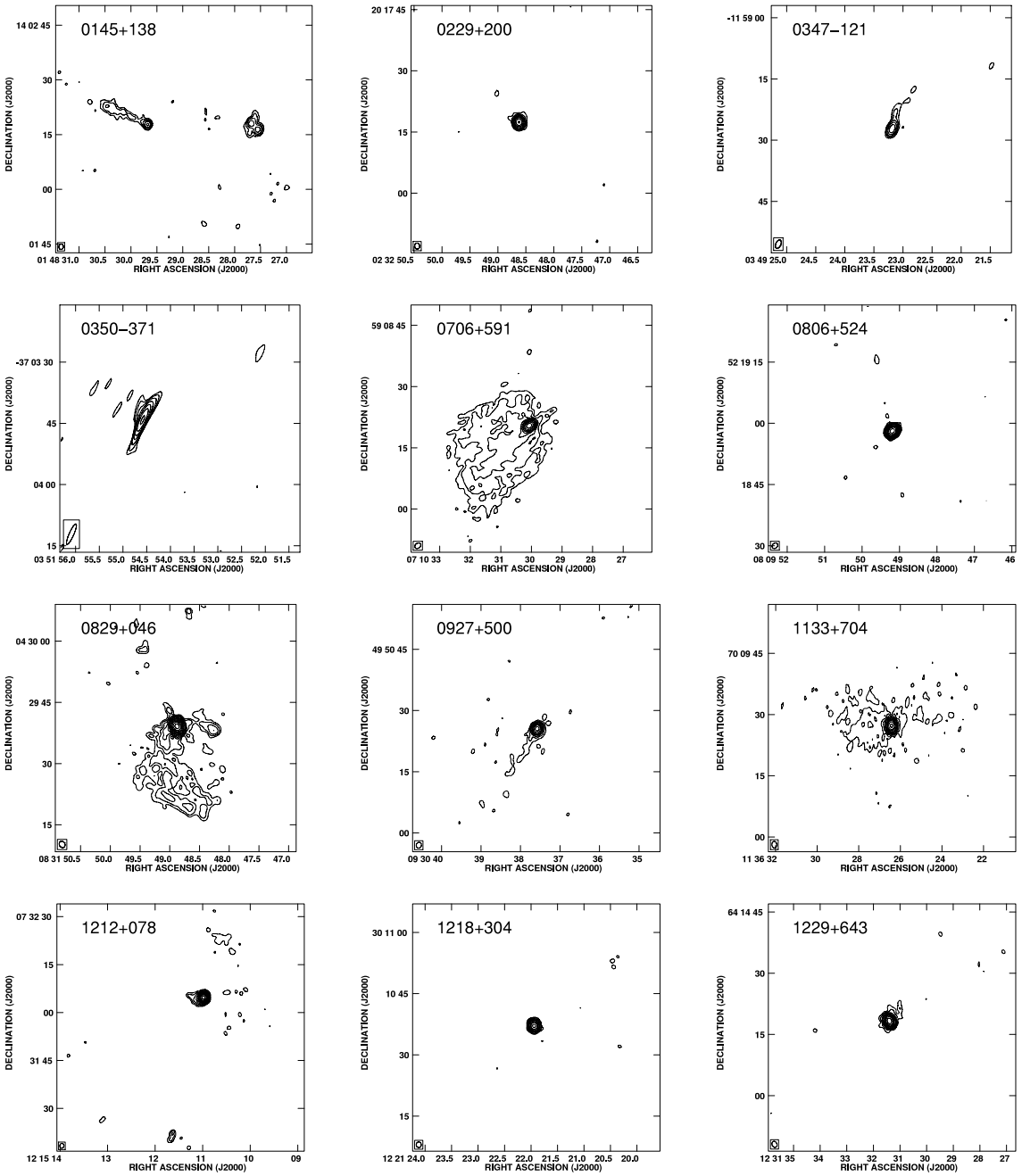

FIG. 2.—VLA images taken in A configuration. Contours are drawn at 1, 2, 4, 8, 16, ... times the noise level. Noise levels and image peaks are given in Table 4.

imported the (u, v) data into DIFMAP (Shepherd et al. 1994, 1995) for further self-calibration and imaging.

4. RESULTS

4.1. *Arcsecond Scale*

We present our final images in Figures 2–5 (see Table 4 for image parameters) and a list of flux densities for all objects in Table 5. We also include low-frequency (325 MHz) data (col. [4]), as measured in the Westerbork Northern Sky Survey (WENSS; Rengelink et al. 1997) or from the Texas Survey (Douglas et al. 1996). For sources lacking flux density measurement from both surveys, we estimate the flux density from the 1.4 GHz NRAO VLA Sky Survey (NVSS; Condon et al. 1998), assuming the average spectral index obtained from other sources, i.e., $\alpha = 0.11$. This is a sensible choice, as all values obtained are below the sensitivity threshold (or out of the sky coverage) of both surveys. For 0521−365 only, whose radio data are missing because of its location, we interpolate the large number of measured fluxes available in the literature from 80 to 8800 MHz. Columns (5) and (6) give the total and core flux densities at 1.4 GHz, and column (7) lists the ratio between these values. We also report the core flux density at 5 GHz in column (8) and the corresponding reference in column (9). Finally, in column (10) we classify sources according to their arcsecond-scale morphology.

For the sake of homogeneity, the total flux densities at 1.4 GHz (col. [5]) are all measured on data from the NVSS. We used, however, information from our higher resolution observations in order to separate possible contribution from

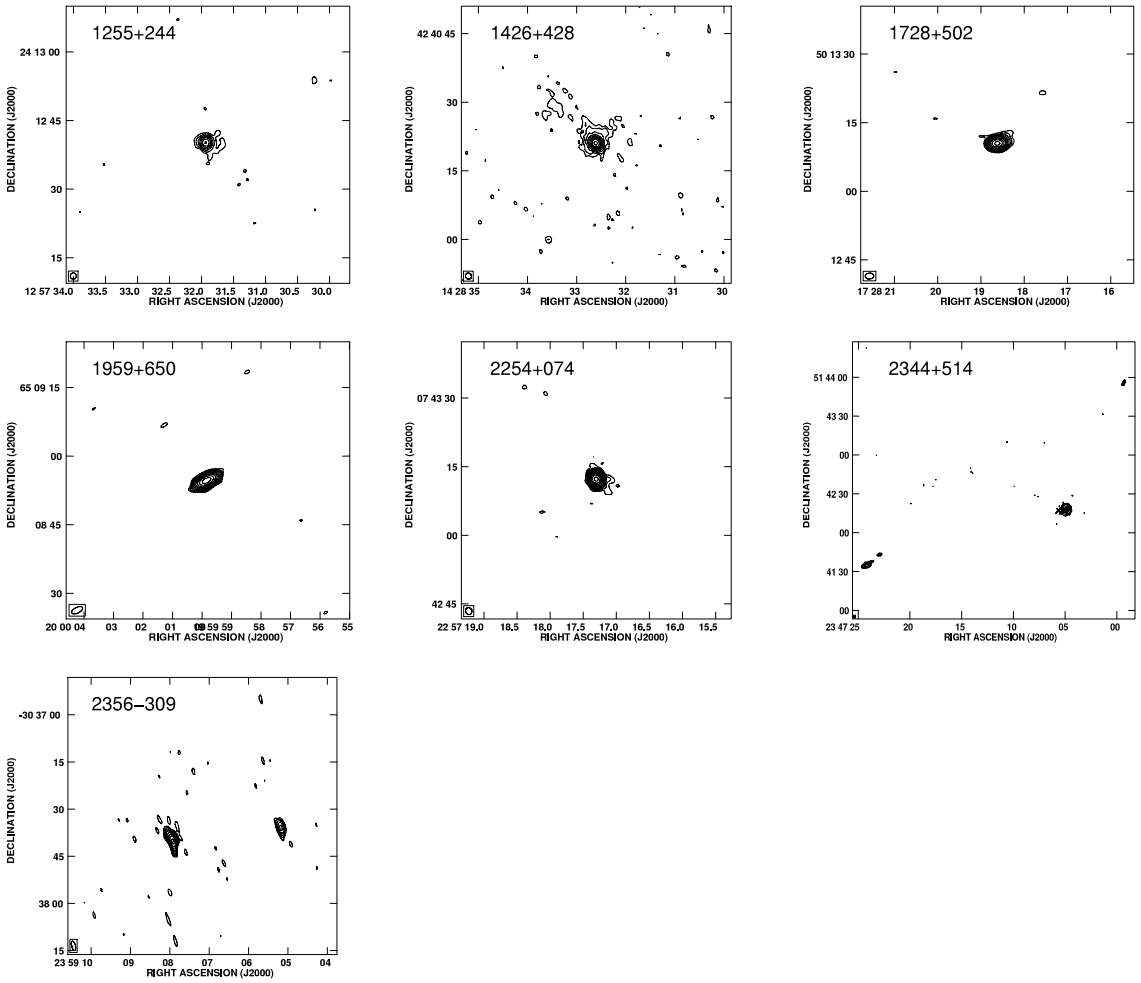

FIG. 3.—Same as Fig. 2, but for additional images.

confusing sources: the A-array images show that this is needed only in 0145+138, in which we subtracted 8 mJy from the NVSS total. For objects also observed in C configuration, we consider the total flux density measured on our images as well and find that the deviation from the NVSS datum is always within ±10%; such a small difference in the total flux density does not affect our results, and it is probably due to core variability effects. In any case, there are no indications that the NVSS systematically overestimates the total flux density. The core value (col. [6]) has been measured using JMFIT in AIPS on our A configuration images (or from the literature, as given in the notes); the corresponding ratio between core and total flux is listed in column (9). In general, the core is the strongest component and accounts for most of the flux. In two objects (1418+546 and 1514−241), the core flux density is even larger than the total; this is probably due to the variability of the core. At the other extreme, there are a number of sources (10/30) where a significant fraction of flux (>50%) is found in extended regions or in secondary components.

We find nine sources where the core is the dominant component: eight objects with a core-jet morphology; four with a core-halo morphology; seven objects with more than one compact component—possibly a hot spot or a background source; and two objects (0548−322 and 0829+047) that are located in rich clusters and are clearly wide-angle tail (WAT) radio sources.

The objects span a range in total power of about 2.5 orders of magnitude at 1.4 GHz. The weakest object is 1255+244, which has $\log P_t = 23.88$ W Hz^{-1}, while the most powerful is 0521−365, with $\log P_t = 26.07$ W Hz^{-1}.

4.2. *Milliarcsecond Structure*

On VLBI scales, our 5 GHz observations have a typical resolution of ∼3.8 mas × 1.5 mas and noise level of a few 0.1 mJy beam^{-1}. Figure 6 presents the images; Table 6 summarizes the most significant parameters: peak flux densities, total intensity, presence of a jet, and jet position angle (P.A.).

All objects are dominated by a strong compact component. In five sources this component is responsible for all the correlated flux density, and in two cases (0548−322 and 1440+122) there is little (∼10%) flux density in extended structures that we could not image. Short one-sided jets (typically <10 mas) are present in seven sources, and only 0521−365 presents a longer jet; in any case, the core is always the strongest component. No counterjet is detected in any of the sources.

We have model-fitted the visibilities of all the sources in DIFMAP. In most cases, we need only one component (in addition to the core) to describe the jet. When two or more components are required, they usually align on a straight path, without showing significant bending. However, a comparison to the largest scale structure indicates that some bending occurs at large distances from the core.

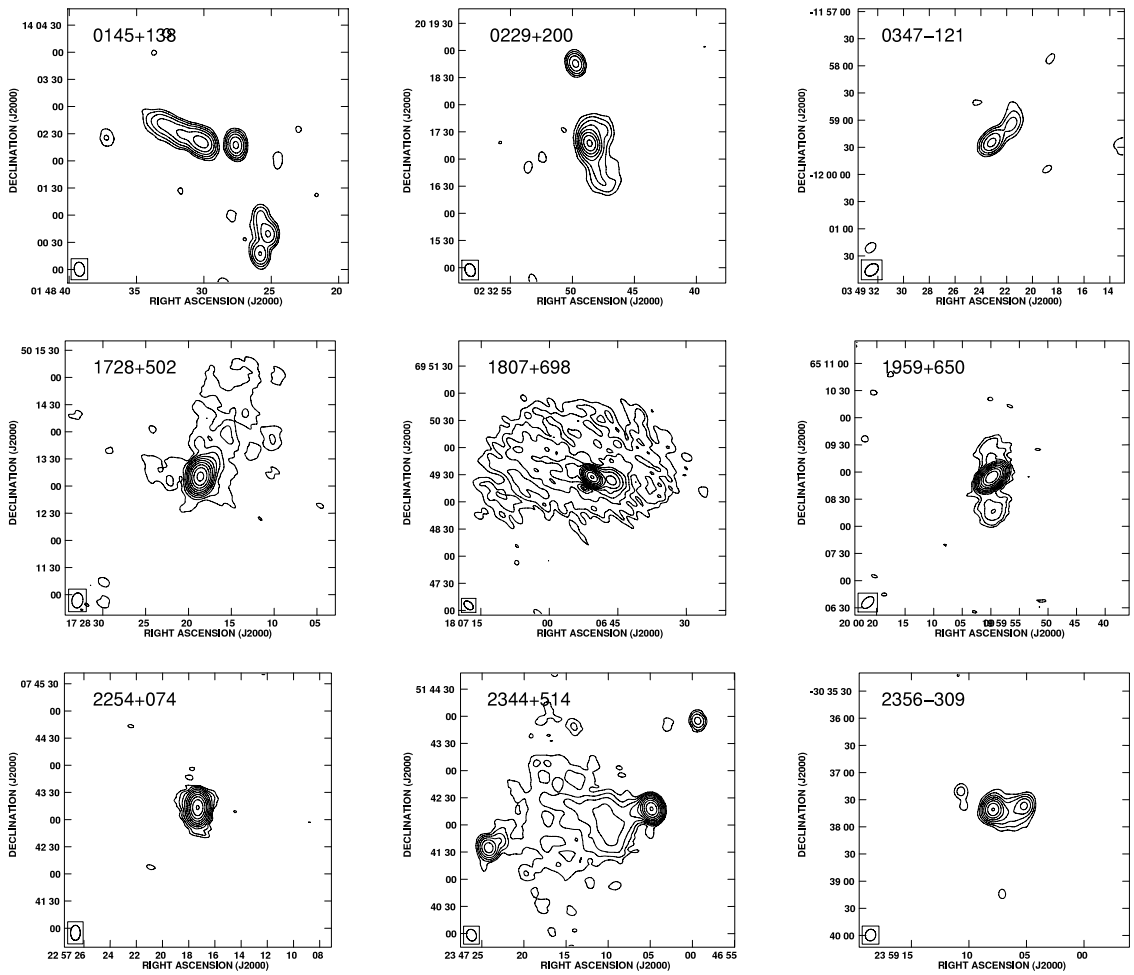

FIG. 4.—VLA images taken in C configuration. Contours are drawn at 1, 2, 4, 8, 16, ... times the noise level. Noise levels and image peaks are given in Table 4.

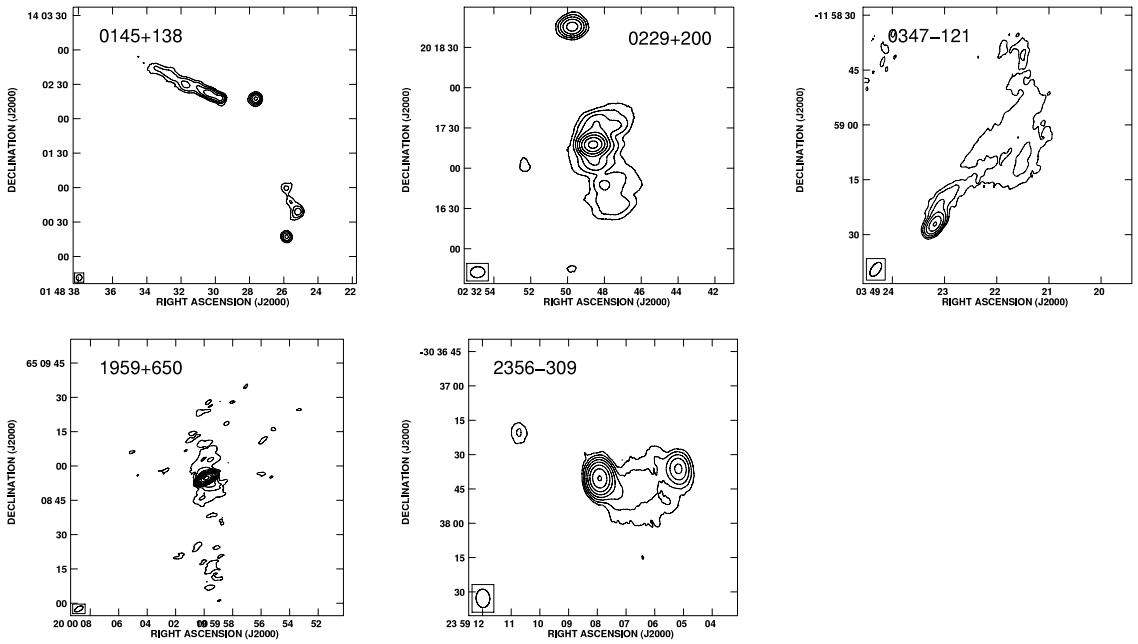

FIG. 5.—VLA images made from a combination of data from the A and C configurations.

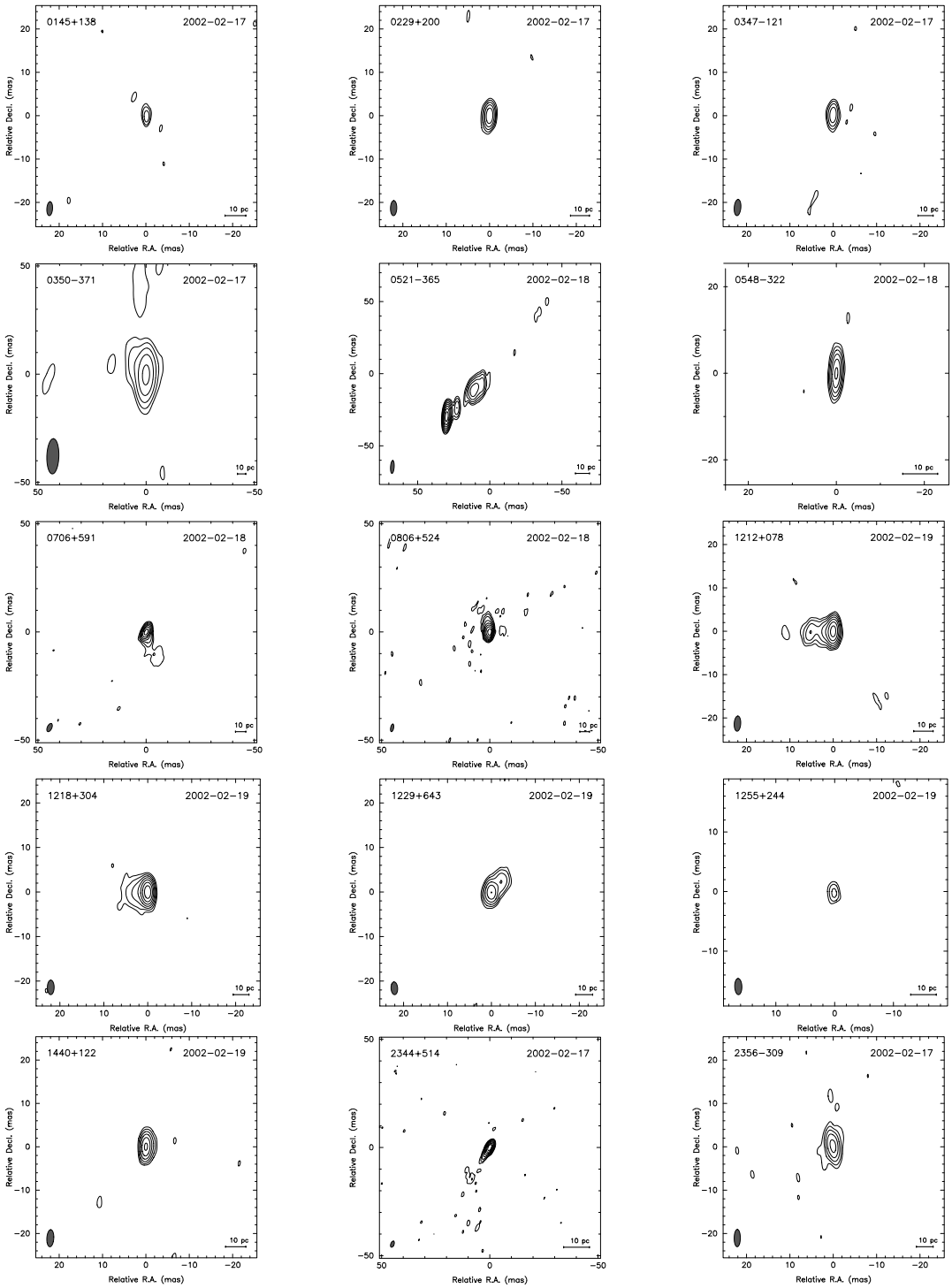

FIG. 6.—VLBA images. Contours are drawn at 1, 2, 4, 8, 16, . . . times the noise level. Noise level and image peaks are given in Table 4.

Finally, from our model fit we determine the jet brightness B_j and the jet/counterjet ratio $R_{\rm min}$, which are presented in columns (7) and (9) of Table 6. Since no object in the sample has a detectable counterjet, the values presented are only lower limits based on the noise of the images. This is also true for objects with values derived from literature data (see notes to Table 6).

4.3. *Parsec/Kiloparsec Scale Comparisons*

A comparison of the morphology on parsec and kiloparsec scales reveals a good agreement in general, and objects in the present sample do not exhibit large bending between small and large scales. There are 10 sources that bend $\leq 30^\circ$, two between 30° and 60°, and two more have bends greater than 60°; for the others there is no preferred direction on either parsec or kiloparsec scales. Even with this uncertainty, this result seems to support the view proposed by Rector et al. (2003), i.e., that HBLs tend to have less bent jets than LBLs (see Fig. 7 and § 5 for discussion). It is also worth noting that all three objects showing an optical and X-ray jet (0521−365, 1807+698, and 2201+044: all LBLs) present straight jets as well. Therefore, with few exceptions, it seems that large bending

TABLE 4
IMAGE PARAMETERS

		VLA (A CONFIGURATION)		VLA (C CONFIGURATION)		VLBA	
NUMBER (1)	NAME (2)	Noise (3)	Peak (4)	Noise (5)	Peak (6)	Noise (7)	Peak (8)
1	0145+138	0.15	2.8	0.24	11.2	0.55	3.5
2	0229+200	0.30	40.4	0.35	52.9	0.49	15.7
3	0347−121	0.30	8.7	0.50	10.4	0.53	7.7
4	0350−371	0.30	22.3	...	...	0.72	11.9
5	0521−365	...	...	...	...	5.50	1034.9
6	0548−322	...	...	...	...	0.90	33.3
7	0706+591	0.15	62.6	...	...	0.38	33.2
8	0806+524	0.20	157.6	...	...	0.38	78.9
9	0829+046	0.25	736.2	...	...	...	...
10	0927+500	0.11	19.9	...	...	...	...
12	1133+704	0.18	111.6	...	...	...	...
13	1212+078	0.12	83.2	...	...	0.36	33.1
15	1218+304	0.20	65.6	...	...	0.41	44.1
16	1229+643	0.12	53.0	...	...	0.61	19.6
17	1255+244	0.10	6.5	...	...	0.55	2.9
19	1426+428	0.10	31.9	...	...	...	...
20	1440+122	...	...	...	...	0.47	17.1
23	1728+502	0.30	201.0	0.30	196.7	...	...
24	1807+698	...	...	0.60	1348.8	...	...
25	1959+650	0.25	198.5	0.24	241.2	...	...
28	2254+074	0.30	407.0	0.90	490.4	...	...
29	2344+514	0.30	195.8	0.40	220.2	0.39	89.7
30	2356−309	0.25	39.2	0.30	40.2	0.66	14.2

NOTES.—Noise levels and peak flux densities for Figs. 2 and 3 (cols. [3] and [4]), for Fig. 4 (cols. [5] and [6]), and for Fig. 6 (cols. [7] and [8]). All units are mJy beam^{-1}.

in BL Lac objects is not common; this agrees with the expectations of unified models, given the findings of Giovannini et al. (2001) that FR I radio galaxies show a good agreement between parsec- and kiloparsec-scale jet P.A. Large bending in the jets is also unlikely in those objects presenting a core+halo morphology, such as 1133+704, 1215+303 (see *FIRST* image; Becker et al. 1995), 1426+428, 1807+698, and 2344+514. The classic explanation is that the halos are lobes seen end-on, and the main axis of the object is closely aligned with the line of sight. This explanation argues against large bends in the jet in these sources as well.

In the comparison between the arcsecond core at 5 GHz and the correlated VLBI flux at the same frequency (given in Tables 5 and 6, respectively) there is a continuity of behavior—only nine sources have integrated VLBI flux densities $\leq$60% of their arcsecond core flux density. This result suggests that only a small fraction ($\sim$30%) of BL Lac objects have a complex subarcsecond structure not visible in our data. In the majority we can follow the structure from parsec to kiloparsec scales.

Observational data suggest that beaming effects play a major role on the parsec scale and become less important on larger (kiloparsec) scales. One clear piece of evidence is the presence of the symmetric structure on the kiloparsec scale in sources with an asymmetric parsec-scale morphology. In sources discussed here we have five sources where VLA images suggest/show the presence of symmetric structure. They are 0229+200, 0706+591, 0829+046, 1807+698, and 1959+650. These results imply that at a projected distance of 5–10 kpc from the core, the jet velocity is no longer relativistic. On the contrary, some sources are still asymmetric in the VLA images. They are 0145+138, 0347−121, 0927+500, and 1212+078. Assuming intrinsically symmetric jets and Doppler favoritism as the origin of observed asymmetries, the radio jets of these sources are still relativistic on scales of tens of kiloparsecs.

4.4. *Notes on Individual Sources*

0145+138.—This is one of the weakest objects ($\log P_{\rm tot,1.4\,GHz} = 24.19$ W Hz^{-1}) to show a core-jet structure. The jet is unusually long for such a low-power object, as it extends for $\sim$200 kpc eastward. On the opposite side of the core, $\sim$25″ westward, there is a secondary component, which is associated with an elliptical galaxy with the same redshift, as previously noted by Perlman et al. (1996; see also Slinglend et al. 1998); our A-array image resolves this source into a double. Other nearby sources are possibly related to the foreground galaxy cluster A257. Note that the total flux given in Table 5 refers to the BL Lac source only; the contribution of the nearby source has been subtracted. The VLBA image shows only a 3 mJy core in agreement with the core flux density from the VLA in A configuration. We surmise that most of the flux density in this source is from the long, one-sided jet.

0229+200.—The C-array image suggests, and the A+C image confirms, the presence of a two-sided jet, with the main jet pointing to the south, in agreement with Rector et al. (2003). About 100″ to the north, we find a compact radio source not yet identified optically. The flux density of the VLBI core is $\sim$16 mJy; no jet is visible on the parsec scale. Thanks to a longer exposure and better (u, v) coverage, the VLBA image by Rector et al. (2003) shows a parsec-scale jet, well aligned with the kiloparsec-scale main jet.

0347−121.—This object shows in the A-array image a jet at P.A. -12°; at 7″ from the core the jet bends by $\sim 35^\circ$ and

TABLE 5
FLUX DENSITIES

Number (1)	Name (IAU) (2)	z (3)	$S_{325\ \mathrm{MHz}}$ (mJy) (4)	$S_{t,1.4\ \mathrm{GHz}}$ (mJy) (5)	$S_{c,1.4\ \mathrm{GHz}}$ (mJy) (6)	c/tot (7)	$S_{c,5\ \mathrm{GHz}}$ (mJy) (8)	Reference (9)	Morphology (10)
1	0145+138	0.125	42 ± 8[a]	35.8	3	0.08	2.1	1	j
2	0229+200	0.140	110 ± 22[a]	94.2	42	0.44	45	1	x
3	0347−121	0.188	30 ± 6[a]	25.7	9	0.35	8.4	1	j
4	0350−371	0.165	46 ± 9[a]	40.1	23	0.57	17	2	c
5	0521−365	0.055	42920 ± 480[b]	17620	3124[c]	0.18	2581	3	x
6	0548−322	0.069	1463 ± 293[d]	505	76[e]	0.15	68	4	w
7	0706+591	0.125	371 ± 3.8	160	65	0.41	80	5	j
8	0806+524	0.137	165 ± 4.1	183	160	0.87	172	1	c
9	0829+046	0.180	671 ± 31[d]	1257	643[c]	0.51	1230	6	w
10	0927+500	0.188	12 ± 3.7	22.3	21	0.94	18	1	c
11	1101+384	0.031	1374 ± 3.3	889	548[e]	0.62	640	7	j
12	1133+704	0.046	529 ± 5.2	337	115	0.34	125	8	h
13	1212+078	0.136	175 ± 35[a]	150	85	0.57	91	1	c
14	1215+303	0.130	1175 ± 2.9	593	355[c]	0.60	445	9	h
15	1218+304	0.182	82 ± 2.7	71.3	67	0.94	56	9	c
16	1229+643	0.164	72 ± 3.7	63	55	0.87	42	10	c
17	1255+244	0.141	19 ± 4[a]	16.6	6.5	0.39	6.9	1	c
18	1418+546	0.152	962 ± 3.4	835	1058[c]	1.27	1189	11	x
19	1426+428	0.129	64 ± 3.1	61.3	32	0.52	22	8	h
20	1440+122	0.162	80 ± 16[a]	68.5	60	0.87	41	1	c
21	1514−241	0.049	1792 ± 43[d]	2177	2562[c]	1.18	1480	12	x
22	1652+398	0.034	1936 ± 4.7	1630	1376[c]	0.84	1250	7	j
23	1728+502	0.055	317 ± 4.2	232	200	0.86	134	8	j
24	1807+698	0.051	4015 ± 4.4	2129	1350[c]	0.63	1507	13	h
25	1959+650	0.048	252 ± 3.5	260	200	0.77	252	1	j
26	2200+420	0.070	1819 ± 4.1	6250	3310[c]	0.53	4857	9	x
27	2201+044	0.027	1222 ± 58[d]	835	179[c]	0.21	168	8	j
28	2254+074	0.190	405 ± 25[d]	404	405	1.00	1216	9	c
29	2344+514	0.044	569 ± 4.2	410	196	0.48	212	1	x
30	2356−309	0.165	75 ± 15[a]	66.2	39	0.59	29	5	x

NOTES.—Col. (4): Total source flux density at 325 MHz from the WENSS, except as noted. Col. (5): Total source flux density at 1.4 GHz from the NVSS. Col. (6): Arcsecond core flux density at 1.4 GHz from VLA A configuration data. Col. (7): Ratio between core and total flux density at 1.4 GHz. Col. (8): Arcsecond core flux density at 5 GHz, with references as given in Col. (9). Col. (10): (c) unresolved, (j) core+jet(s), (h) core+halo, (x) extended, complex structure, and (w) wide-angle tail.

[a] Extrapolated from the 1.4 GHz flux density (col. [5]) with $\alpha = 0.11$.

[b] Interpolated from NED data between 80 and 8800 MHz.

[c] Antonucci & Ulvestad (1985).

[d] Texas Survey (Douglas et al. 1996).

[e] Laurent-Muehleisen et al. (1993).

REFERENCES.—(1) Perlman et al. 1996; (2) Veron-Cetty & Veron 1993; (3) interpolated from data between 1.4 and 15 GHz; (4) Reid et al. 1999; (5) NED; (6) MERLIN archive data; (7) Giovannini et al. 2001; (8) Laurent-Muehleisen et al. 1993; (9) Fossati et al. 1998; (10) Padovani & Giommi 1995; (11) Murphy et al. 1993; (12) Morganti et al. 1993; (13) Cassaro et al. 1999.

expands with a large opening angle, showing in the A+C image a lobelike structure. The VLBI image gives no indication of a parsec-scale jet.

0350−371.—Because of its low declination (decl. $= -37^\circ$), this object has a somewhat lower resolution A configuration image. There is an indication of a jet present on both arcsecond and milliarcsecond scales, as an elongation of the main component to the northeast at P.A. 33° and 46°, respectively. This yields a small bend of ΔP.A. $\sim -13^\circ$ from the parsec to the kiloparsec scale.

0521−365.—This is a nearby ($z = 0.055$) bright EGRET source (Lin et al. 1995). The optical spectrum of this object exhibits prominent and variable emission lines (Scarpa et al. 1995), and it was also classified as an N galaxy and a Seyfert galaxy, although its host galaxy is a luminous giant elliptical galaxy (Falomo 1994). This source is also well known for the presence of a prominent radio and optical jet (Danziger et al. 1979; Keel 1986; Falomo 1994), which resembles that of the nearby radio galaxy M87 (i.e., Sparks et al. 1994). The optical jet is well aligned with the kiloparsec radio jet, and the radio and optical structures have a clear correspondence (Scarpa et al. 1999). Our VLBA image shows that the same P.A. found on the parsec-scale jet is maintained, without any significant bending, over 3 orders of magnitude. This is consistent with a relatively large angle of view, in agreement with the absence of superluminal motion showed by Tingay & Edwards (2002) and the findings of Pian et al. (1996).

0548−322.—This southern object resides in a rich environment, with close companions and other galaxies at the same redshift (Falomo et al. 1995). This is in agreement with the WAT structure revealed on kiloparsec scales by Laurent-Muehleisen et al. (1993) and Reid et al. (1999). The parsec-scale image is dominated by a 35 mJy core, with little or no other emission detected. The large difference between this value and the kiloparsec total flux density suggests that the emission on large scales is spread over an extended low-brightness area.

TABLE 6
VLBA Data at 5 GHz

Number (1)	Name (2)	z (3)	S_t (mJy) (4)	S_c (mJy) (5)	$S_{t,\mathrm{mas}}/S_{c,''}$ (6)	B_j (mJy beam^{-1}) (7)	P.A.$_{\mathrm{jet}}$ (deg) (8)	R ($\geq$) (9)	$\beta\cos\theta$ ($\geq$) (10)	Reference (11)
1	0145+138	0.125	3.3	3.2	1.61	...	...	...	...	1
2	0229+200	0.140	18.2	17.0	0.40	...	...	...	...	1
3	0347−121	0.188	8.5	8.1	1.01	...	...	...	...	1
4	0350−371	0.165	16.9	14.0	0.99	2.40	46	8	...	1
5	0521−365	0.055	1747	995.0	0.68	142.5	−44	119	0.74	1
6	0548−322	0.069	41.7	36.3	0.61	...	...	...	...	1
7	0706+591	0.125	42.0	33.8	0.53	3	−158	25	...	1
8	0806+524	0.137	136.8	66.0	0.80	40	20	333	0.82	1
9	0829+046	0.180	740	440.0	0.60	90	65	90	...	2
10	0927+500	0.188	...	...	...	...	...	...	...	
11	1101+384	0.031	400	200	0.63	10	−32	100	0.73	3
12	1133+704	0.046	137.9	82.7	1.10	9.5	105	16	...	4
13	1212+078	0.136	50.0	34.5	0.53	3.0	92	23	...	1
14	1215+303	0.130	372.0	276.0	0.84	9.4	140	157	0.77	3
15	1218+304	0.182	56.9	39.8	1.02	3.2	73	25	...	1
16	1229+643	0.164	35.7	26.9	0.85	5.0	−43	28	...	1
17	1255+244	0.141	2.8	2.8	0.40	...	...	...	...	1
18	1418+546	0.152	1090	209.0	0.92	40	120	40	...	5
19	1426+428	0.129	21.2	19.1	0.96	2.1	20	3	...	4
20	1440+122	0.162	18.5	17.2	0.45	...	...	...	...	1
21	1514−241	0.049	2278	1948	1.49	253	161	90	...	6
22	1652+398	0.034	1118	491	0.89	100	150	400	0.83	7
23	1728+502	0.055	171	110.0	1.28	18.0	−55	200	0.79	3
24	1807+698	0.051	780	560.0	0.52	50	−102	38	...	2
25	1959+650	0.048	220	181.7	0.87	1.6	−5	8	...	8
26	2200+420	0.070	2164	1148	0.45	300	−170	350	0.82	9
27	2201+044	0.027	170	131.3	1.01	3.0	−42	3	...	4
28	2254+074	0.190	350	280.0	0.29	38.4	−120	43	...	2
29	2344+514	0.044	116.7	70.0	0.55	3.0	142	25	...	1
30	2356−309	0.165	21.9	21.9	0.76	...	...	...	...	1

Notes.—Col. (4): Correlated VLBI flux density at 5 GHz. Col. (5): VLBI core flux density. Col. (6): Ratio between total VLBI flux density and arcsecond core at 5 GHz (col. [8] in Table 5). Col. (7): Jet brightness near the core. Col. (8): Jet P.A. Col. (9): Lower limit for the jet/counterjet ratio. Col. (10): Estimated lower limit for $\beta\cos\theta$.

References.—(1) Present work; (2) Fey & Charlot 2000; (3) M. Giroletti et al. 2004, in preparation, (4) Kollgaard et al. 1996; (5) Cassaro et al. 2002; (6) Fomalont et al. 2000; (7) Giroletti et al. 2004; (8) Rector et al. 2003; (9) Gabuzda & Cawthorne 2003.

0706+591.—Our image in A configuration is a significant improvement in resolution with respect to the only image published so far (Laurent-Muehleisen et al. 1993). The main structure is quite extended and broad, and the core is located at the northwest edge of this quite round cocoon. It could be a tailed radio structure (WAT or narrow-angle tail [NAT]) viewed at a small angle of sight. Note, however, that there is no indication of an overdensity of galaxies in its vicinity. A small orientation angle is also suggested by the different direction of the parsec-scale core-jet structure (ΔP.A. $\sim 80^\circ$).

0806+524.—This source is heavily core-dominated. It looks pointlike with the VLA, with a flux density of 160 mJy beam^{-1} at 1.4 GHz. On the VLBI scale, the integrated flux density at 5 GHz is 137 mJy, distributed in a core, and a short ($\sim$5 mas) northbound (P.A. $\sim 13^\circ$) jet.

0829+046.—This is one of the rare BL Lac objects in which there is evidence of emission on both sides of the core. In the VLA A-array image, two symmetric jets emerge at P.A. 110° and -70°. Both jets bend, showing a radio structure typical of head-tail radio galaxies. For this reason, we believe that the large bending of the jet is related to this motion and not intrinsic to the source (see also Antonucci & Ulvestad 1985). This leaves us with a bend between parsec and kiloparsec scales of 44° (see the VLBA image in Jorstad et al. 2001; Fey & Charlot 2000; Lister et al. 1998).

0927+500.—This is the second most distant source in the sample and looks like a faint ($\sim$20 mJy) core-dominated source. No information is available on the parsec-scale morphology.

1133+704.—Our observation reveals a core-halo morphology, confirming the claim of Wardle et al. (1984). The halo is faint and heavily resolved in the image in A configuration. This explains the results of Laurent-Muehleisen et al. (1993): in their 5 GHz image, the halo is resolved out, and only the compact 125 mJy core is detected. The major axis of the halo is in the east-west direction, i.e., well aligned with the parsec-scale jet detected by Kollgaard et al. (1996).

1212+078.—This object presents a good alignment between the parsec- and kiloparsec-scale structure. The jet is oriented at $\sim 90^\circ$ and is detected for 12 mas with the VLBA and almost $50''$ with the VLA. Rector et al. (2003) present a VLBA image (1997 May 17) and a deep B-array VLA image, suggesting a transverse orientation for the extended structure. A compact feature 40 mas south of the core is present in our image as well as in that of Rector et al. (2003). It is likely that our VLA image resolves some of the extended emission, which is also visible in Perlman et al. (1996) on the opposite side, as well as in the *FIRST* and NVSS images.

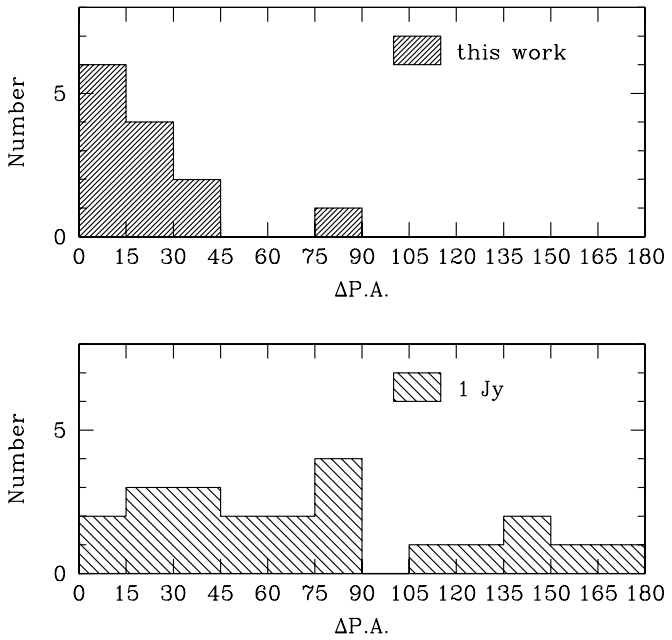

FIG. 7.—Distribution of bending for sources in the present sample (*top*) and in the 1 Jy sample (*bottom*; see text). We have excluded from our sample objects belonging to the 1 Jy sample.

1218+304.—We confirm that this source is compact on kiloparsec scales (see Perlman 1994; Laurent-Muehleisen et al. 1993 and references therein) and place an upper limit on its size of 0.″19; at the redshift of 1218+304 ($z = 0.182$; E. S. Perlman et al. 2004, private communication), this corresponds to 0.7 kpc. The VLBA image reveals a 10 mas jet emerging at P.A. $\sim 90^\circ$. The total VLBA correlated flux is 57 mJy and dominates the total flux density of the source.

1229+643.—The kiloparsec-scale structure shows an almost unresolved core (see also Perlman 1994), with a little emission from a halo-like feature. However, even if the poor signal-to-noise ratio of this structure does not allow us to make any strong claim about its nature, we can estimate that it is oriented at a P.A. of about -20°. This is in general agreement with the previous image from Perlman & Stocke (1993). The VLBA jet points northwest (P.A. $= -43^\circ$), and the core-jet structure accounts for most of the flux density from this source. Therefore, we tentatively propose a ΔP.A. $\lesssim 25^\circ$.

1255+244.—This extremely weak object is only marginally resolved with the VLA and barely detected by the VLBA ($\sim$3 mJy core). This is the weakest object in the sample ($\log P_{\rm tot,1.4\,GHz} = 23.5$ W Hz^{-1}).

1426+428.—The comparison of the NVSS total flux density (61 mJy) and the peak of the A-array image (32 mJy beam^{-1}) indicates that some extended emission is present. Our image confirms the presence of a faint halo surrounding the central core but does not recover all the flux. Since previous images in the C array (Laurent-Muehleisen et al. 1993) detected an intermediate value of 46 mJy, we believe that the difference has to be ascribed to resolution effects rather than variability. The northwest extension is oriented at P.A. $\sim 50^\circ$ and therefore presents a ΔP.A. $= 30^\circ$ with respect to the inner structure studied by Kollgaard et al. (1996). Note that this is a TeV source (Aharonian et al. 2002; Horan et al. 2002).

1440+122.—Little information can be obtained for this object. The VLBA image reveals only a faint (15 mJy) core, possibly extended to the west. VLA images obtained by Giovannini et al. (2004) show a nuclear flat spectrum nuclear emission surrounded by a steep-spectrum halo structure $\sim 8''$ in size at 8.4 GHz moderately elongated in the southwest direction.

1728+502.—The 200 mJy core dominates the source; it is slightly resolved to the northwest in the A configuration image. The C-array VLA image detects $\sim$16 mJy of extended emission in the same direction (at P.A. -30°), spread over more than 100″. A bending of $\sim 25^\circ$ west is required from the parsec-scale jet shown by VLBA (Kollgaard et al. 1996) and EVN+MERLIN images (M. Giroletti et al. 2004, in preparation).

1807+698.—This is a well-known source (3C 371), with a jet detected in the optical with *HST* (Scarpa et al. 1999) and in the X-rays with *Chandra* (Pesce et al. 2001). This jet does not bend significantly and is well aligned (at P.A. $\sim 100^\circ$) with the parsec-scale jet imaged with the Space VLBI by Gómez & Marscher (2000). The orientation is in good agreement with the P.A. of the jet visible in our C-array image (ΔP.A. consistent with 0) and of the main lobe detected in the deep B-array image at 5 GHz by Wrobel & Lind (1990); see also the 5 and 15 GHz VLA observations of O'Dea et al. (1988). Thanks to the lower frequency and more compact configuration, we also detect a diffuse halo of about 340 mJy, surrounding both lobes and extending over 200″ (see also Cassaro et al. 1999).

1959+650.—Costamante & Ghisellini (2002) suggested that this object could be a TeV source; in fact, a strong detection of very high energy γ-rays was obtained with the Whipple 10 m telescope (Holder et al. 2003) and the HEGRA Cerenkov telescopes (Aharonian et al. 2003), confirming the preliminary results presented by Nishiyama et al. (1999). Our C-array radio image clearly shows a peculiar two-sided structure. The combination of A and C data indicates that the symmetry could be in the jet region, suggesting that the source is oriented in the plane of the sky and/or that the jet is nonrelativistic on the arcsecond scale. The parsec-scale jet in the image by Rector et al. (2003) at 5 GHz has a P.A. of -5°, indicating that the jet does not change direction over 3 orders of magnitude. Note, however, that high-frequency (15 GHz) observations suggest a 1 mas jet to the southeast, at P.A. $\sim 160^\circ$ (Piner & Edwards 2004).

2254+074.—This source has one of the brightest cores ($\log P_{c,\,5\,\rm GHz} = 26.1$ W Hz^{-1}). Only a little extended emission is present on the arcsecond scale, both in the A and C configurations. A comparison to the parsec-scale total flux density (350 mJy; Fey & Charlot 2000) indicates that some emission originates on intermediate scales.

2344+514.—This is one of the most puzzling sources in the sample. VLA images show two bright components within 200″ (180 kpc) from the position of the optical and radio core. Furthermore, extended low-brightness emission is present between the core and the eastern feature. The A-array observation resolves the faint emission, revealing a core-halo morphology, while the eastern feature appears extended in the direction of the core. Since this extension is also visible in the C-array image (as well as in the B-array map of Rector et al. 2003), it cannot be ascribed to bandwidth smearing. This elongation and the diffuse radio bridge connecting it to the core indicates that the component is related to the source. On the contrary, the northwest component does not show any radio structure suggesting a connection. Finally, the VLBA image shows a jet oriented at 142° (see also Rector et al. 2003), confirming the complexity of this source (ΔP.A. $\sim 45^\circ$ to the VLA main axis). Note also that Catanese et al. (1998) report a TeV detection from this source and that *Chandra*

observations reveal diffuse X-ray emission in its environment (Donato et al. 2003).

2356−309.—Two components separated by 36″ are connected by a weaker "bridge," resolved by the VLA in A configuration. A third component is found on the opposite side. The core is barely detected on the parsec scale because of the low declination (−30°) and flux density (21 mJy) of this BL Lac object. Because of the presence of a core, a radio bridge, and two possibly related compact structures, this source is similar to 2344+514.

5. DISCUSSION

According to the current view of the unification of AGNs, BL Lac objects are expected to be FR I radio galaxies oriented at a small angle with respect to the line of sight. Moreover, radio data (e.g., Giovannini et al. 2001) as well as variability, one-sidedness, superluminal motion, and high-frequency emission (X-rays and γ-rays) strongly support the existence of relativistic jets. In agreement with the presence of fast jets and small angles to the line of sight, BL Lac objects are usually core-dominated objects. However, we note that in our sample we have 10/30 objects in which the core flux density is less than 50% of the total flux density at 1.4 GHz.

Under the standard assumption that jets are intrinsically symmetric, we can derive constraints on the jet velocity and orientation. The approaching jet is amplified by relativistic beaming, and the counterjet is deboosted. The observed ratio R between the observed jet and counterjet brightness is related to the intrinsic jet velocity β and orientation angle θ by $R = [(1 + \beta\cos\theta)/(1 - \beta\cos\theta)]^p$, where $p = 2 + \alpha$ (continuous jet) or $p = 3 + \alpha$ (moving sphere). Here we assume a continuous jet, with spectral index $\alpha = 0.5$ [$S(\nu) \propto \nu^{-\alpha}$], following Giovannini et al. (1994) and references therein.

However, in BL Lac objects the counterjet is generally deboosted below the detection threshold on the parsec scale and we can only determine lower limits $R_{\rm min}$. Furthermore, since our sample is dominated by faint objects, the main jet shows in most cases a low-brightness emission resulting in a small $R_{\rm min}$. Therefore, in most cases we do not find significant constraints on β and θ; the jet/counterjet ratio is $R_{\rm min} > 100$ in only six objects. In these cases, we give the relative limits on $\beta\cos\theta$ in Table 6 (col. [10]).

The relativistic boosting at the base of the jet affects the observed radio power of the core; by comparing this value to that expected from the total power at low frequency via the correlation found by Giovannini et al. (1988, 2001), we can derive the amount of boosting. We account for variability, which results in a range of possible Doppler factors for each source after allowing for a variation of a factor of 2 in the core flux density. Considering these intervals, we estimate for each object the allowed orientation angle under the assumption of a Lorentz factor $\Gamma = 5$. We note that larger Lorentz factors do not significantly change the permitted angles, while values of $\Gamma < 3$ are not allowed, according to Giovannini et al. (2001) and from strong and widely accepted lines of evidence (superluminal motions, rapid variability, high observed brightness temperatures, and detection of γ-ray emission).

The synchrotron self-Compton model (SSC; Ghisellini et al. 1993) poses a third observational constraint on the Doppler factor by requiring that the X-ray flux produced by inverse Compton scattering does not exceed that observed. Thanks to the availability of a large number of observations carried out by X-ray satellites (*Einstein*, *EXOSAT*, *ROSAT*, *ASCA*, and *BeppoSAX*), Donato et al. (2001 and references therein) have collected fluxes at 1 keV for all the objects in the sample. The standard SSC formula (Marscher 1987) yields the Doppler factor as an inverse power of the VLBI core angular dimension; since VLBI cores are unresolved in our data, we find lower limits on δ. There are 20 sources for which the result is not informative; however, for 11 sources we have mild limits on δ, as reported in Table 7. These limits provide useful constraints on the minimum velocity and the maximum angle allowed. Basically, these values are in good agreement with those required from the core enhancement argument; given the independence of the two estimates, this strengthens the conclusion that small to moderate angles to the line-of-sight and high-velocity jets are characteristic of the objects in the sample.

We illustrate the resulting allowed angles in Figure 8. The derived angles are consistent with the unified scheme, since

TABLE 7

Limits from the Synchrotron Self-Compton Model

Name (1)	$\delta_{\rm min}$ (2)	$\Gamma_{\rm min}$ (3)	$\theta_{\rm max}$ (deg) (4)
0521−365	2.2	1.3	27
0829+046	4.6	2.4	13
1101+384	2.4	1.4	25
1215+303	2.6	1.5	22
1418+546	2.2	1.3	26
1514−241	9.3	4.7	6
1652+398	2.5	1.4	24
1807+698	5.3	2.7	11
2200+420	6.7	3.4	9
2201+044	1.1	1.1	65
2254+074	4.0	2.1	15

Notes.—Col. (2): Minimum Doppler factor from SSC (we only report sources where $\delta_{\rm min} > 1$). Col. (3): Minimum Lorentz factor Γ. Col. (4): Largest possible orientation angle.

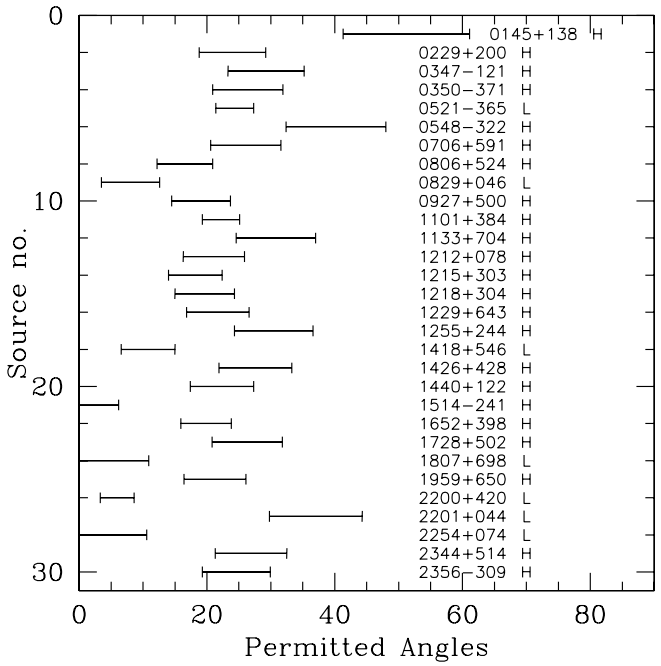

Fig. 8.—Allowed angles to the line of sight, assuming $\Gamma = 5$. The letter beside the name refers to the type of source (H: high-frequency–peaked BL Lac object; L: low-frequency–peaked BL Lac object).

TABLE 8
FINAL INTRINSIC PARAMETERS WITH $\Gamma = 5$

Number (1)	Name (2)	$\log P_t$ (W Hz^{-1}) (3)	$\Delta\theta_5$ (deg) (4)	$\Delta\delta_5$ (5)	$\Delta P_{c,i}$ (W Hz^{-1}) (6)
1	0145+138	24.17	41–61	0.4–0.8	23.10–23.70
2	0229+200	24.69	19–29	1.4–2.8	23.42–24.02
3	0347−121	24.39	23–35	1.0–2.0	23.24–23.84
4	0350−371	24.46	21–32	1.2–2.4	23.28–23.88
5	0521−365	26.45	21–27	1.5–2.3	24.51–24.86
6	0548−322	25.19	32–48	0.6–1.2	23.73–24.33
7	0706+591	25.12	21–32	1.2–2.4	23.69–24.29
8	0806+524	24.85	12–21	2.4–4.7	23.52–24.12
9	0829+046	25.70	3–13	4.6–9.1	24.05–24.65
10	0927+500	23.99	15–24	2.0–3.9	22.99–23.59
11	1101+384	24.46	19–25	1.8–2.7	23.28–23.63
12	1133+704	24.39	25–37	0.9–1.8	23.23–23.83
13	1212+078	24.87	16–26	1.7–3.4	23.53–24.13
14	1215+303	25.65	14–22	2.1–4.0	24.02–24.57
15	1218+304	24.80	15–24	1.9–3.7	23.49–24.09
16	1229+643	24.65	17–27	1.6–3.2	23.40–24.00
17	1255+244	23.93	24–37	0.9–1.9	22.95–23.55
18	1418+546	25.71	7–15	3.7–7.5	24.05–24.65
19	1426+428	24.38	22–33	1.1–2.2	23.23–23.83
20	1440+122	24.68	17–27	1.5–3.1	23.42–24.02
21	1514−241	24.97	0–6	7.7–9.9	22.90–23.11
22	1652+398	24.69	16–24	1.9–3.5	23.42–23.93
23	1728+502	24.32	21–32	1.2–2.4	23.19–23.79
24	1807+698	25.36	0–11	5.3–9.9	22.94–23.48
25	1959+650	24.10	16–26	1.7–3.3	23.06–23.66
26	2200+420	25.29	3–9	6.4–9.2	23.80–24.11
27	2201+044	24.28	30–44	0.7–1.3	23.17–23.77
28	2254+074	25.53	0–11	5.4–9.9	24.02–24.54
29	2344+514	24.38	21–32	1.2–2.3	23.23–23.83
30	2356−309	24.67	19–30	1.3–2.7	23.41–24.01

NOTES.—Col. (3): Logarithm of total radio power at 325 MHz. Col. (4): Range of possible jet orientation angle. Col. (5): Doppler factor range. Col. (6): Logarithm of intrinsic core radio power at 5 GHz.

most of the BL Lac objects in our sample are oriented at a small to moderate angle to the line of sight. In Table 8, we present the resulting best available estimates from the previous studies of the allowed jet orientation angle θ and the relative Doppler factor δ in the case $\Gamma = 5$. We note that despite the low number of LBLs considered here, they seem to be oriented at smaller angles ($\langle\theta\rangle_{\rm LBL} = 14^\circ \pm 12^\circ$) with respect to HBLs ($\langle\theta\rangle_{\rm HBL} = 25^\circ \pm 9^\circ$). A Kolmogorov-Smirnov (K-S) test on the viewing angles for the two populations of HBLs and LBLs yields a probability of less than 8×10^{-3} that the data sets are drawn from the same distribution (K-S statistic $d = 1.66$). Note, however, the rather large uncertainties, which are due not only to the small number of objects but also to a likely large scatter in the distribution of intrinsic angles.

The adoption of a single Lorentz factor can also be partly responsible for this result. Although the assumption of $\Gamma = 5$ is a good approximation of the real situation, we explore another approach, less restrictive than assuming a constant velocity for all the jets. In particular, we consider the relation $\Gamma \sim 1/\theta$, which corresponds to the maximum angle allowed for a given Doppler factor and is, in a statistical sense, the most likely situation. We still make use of the P_{c/P_t} relation in order to uniquely determine the values of β and θ. We show in Figure 9 the histogram of the resulting angles and Lorentz factor distribution. The average angle for the sample is $\langle\theta\rangle = 18^\circ \pm 5^\circ$, without showing any relevant difference between LBLs and HBLs ($\langle\theta_{\rm LBL}\rangle = 15^\circ \pm 7^\circ$ and $\langle\theta_{\rm HBL}\rangle = 20^\circ \pm 4^\circ$, respectively). There are still four LBLs that need to be oriented at rather small angles ($\theta < 15^\circ$), namely, 0829+046 ($z = 0.180$), 1418+546 ($z = 0.152$), 2200+420 ($z = 0.070$), and 2254+074 ($z = 0.190$); however, their redshifts are typically larger than average, so these may be more extreme and peculiar objects. In Figure 9 (*right panel*), we also show the distribution of Lorentz factors: the majority of objects, including all HBLs, are distributed around $\Gamma = 3$. There are, however, four objects separated from the others, which have $\Gamma > 5$; these objects are the four LBLs mentioned above.

Depending on the assumptions made on the jet bulk velocity, we are left with two alternatives on the beaming properties of the jet: either our HBLs are viewed at somewhat larger angles than LBLs, or the bulk velocity of the radio jets for the HBL population is intrinsically smaller. The former explanation has been put forward several times in the literature (e.g., Celotti et al. 1993; Jannuzi et al. 1994), although it cannot satisfactorily account for *all* observed properties of BL Lac objects (Sambruna et al. 1996; Rector & Stocke 2001). Conversely, the latter interpretation has been less explored and is puzzling, since constraints on smaller scales, and from other arguments (e.g., TeV γ-ray emission), require an opposite behavior. However, we note that on parsec scales, the study of proper motions has revealed superluminal components in EGRET sources (Jorstad et al. 2001) and subluminal

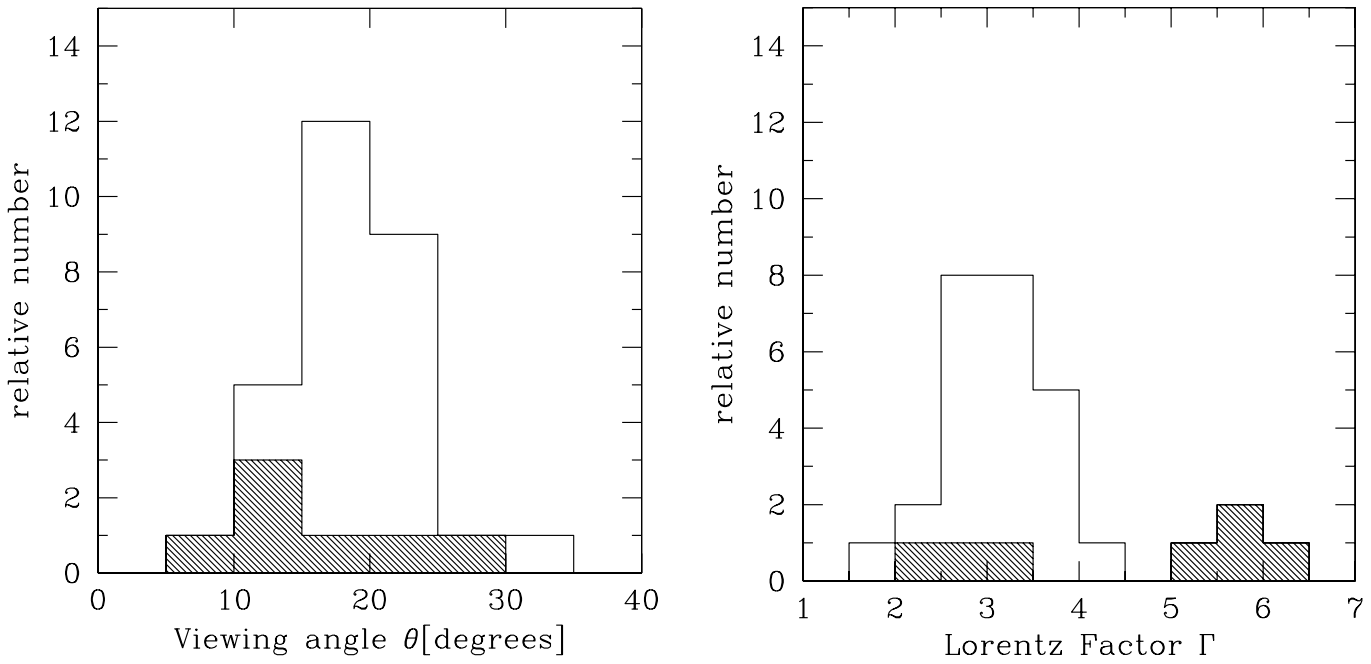

FIG. 9.—Distribution of the resulting viewing angle θ (*left*) and Lorentz factor Γ (*right*), assuming $\Gamma \sim 1/\theta$; the shaded parts correspond to LBLs only.

or absent motion in TeV sources (Tingay & Edwards 2002; Piner & Edwards 2004). Thus, it is interesting to speculate that the emission of TeV photons taking place on even smaller scales may be responsible for energetic losses resulting in slower jets on radio scales. Another possible explanation for the decrease in jet velocity invokes the properties of the ISM, which can vary among galaxies. Note that evidence of a strong jet deceleration within ~5 kpc from the core has been found in 3C 449 (Feretti et al. 1999), 3C 31 (Laing & Bridle 2002), M87 (Biretta et al. 1999), and 3C 264 (Baum et al. 1997; Lara et al. 2004).

Since samples of distant objects with large flux limits (e.g., the 1 Jy) have been studied in detail, it is worthwhile to compare some properties of the two populations. The value of the core dominance parameter $f = S_{\rm core}/S_{\rm ext}$ in our sample is $\langle f \rangle = 3.2$ (see Fig. 10). Actually, we excluded the three sources (1418+546, 1514−241, and 2254+074) in which the flux density of the core is larger than the total; this behavior has to be ascribed to variability and reminds us that this result needs to be considered with caution. However, this is also true for other samples, and we do not expect it to affect the average properties of the sources in our sample. The present low-redshift BL Lac sample is less core-dominated than the Extended Medium-Sensitivity Survey (EMSS) and the 1 Jy; in the EMSS $\langle f \rangle \geq 4.2$ (Rector et al. 2000), and much larger values are observed in the bright 1 Jy BL Lac objects (Rector & Stocke 2001). Correspondingly, the core is frequently associated with a resolved radio morphology, including halos, secondary components, and symmetric two-sided jets; this also suggests that kiloparsec-scale jets may have different

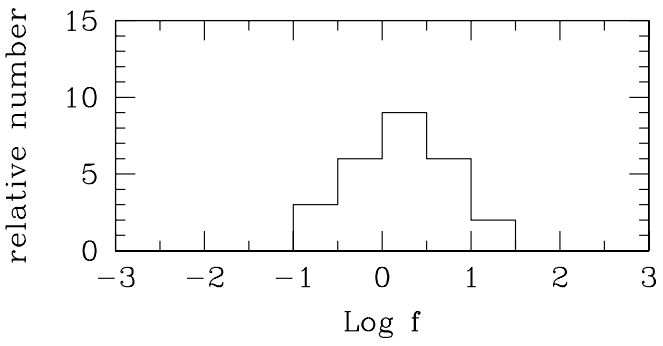

FIG. 10.—Distribution of the core dominance factor f for sources in the present sample.

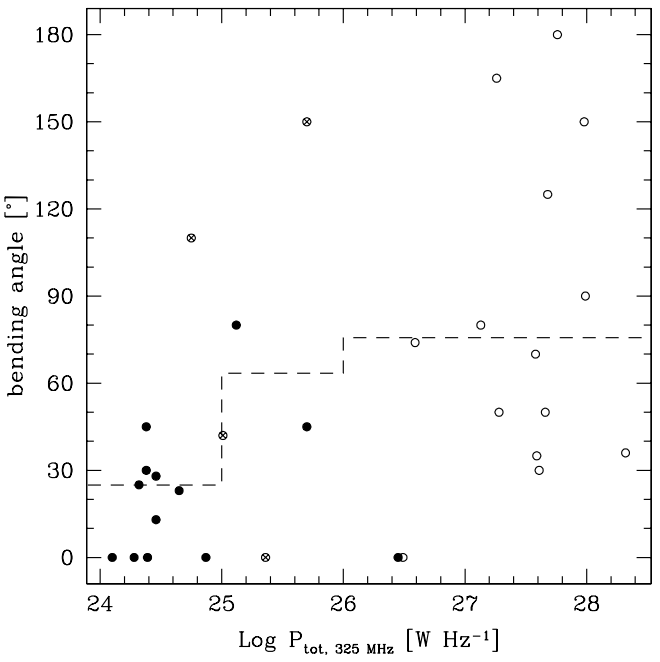

FIG. 11.—Bending angle vs. total radio power at low frequency (325 MHz). The diagram includes both BL Lac objects from the present work (*filled symbols*) and the 1 Jy sample (*open symbols*); the crossed symbols are the four objects common to both samples (1418+546, 1514−241, 1652+398, and 1807+698); the dashed line corresponds to the average bending angle in the three luminosity bins: $24 < \log P < 25$, $25 < \log P < 26$, and $\log P > 26$.

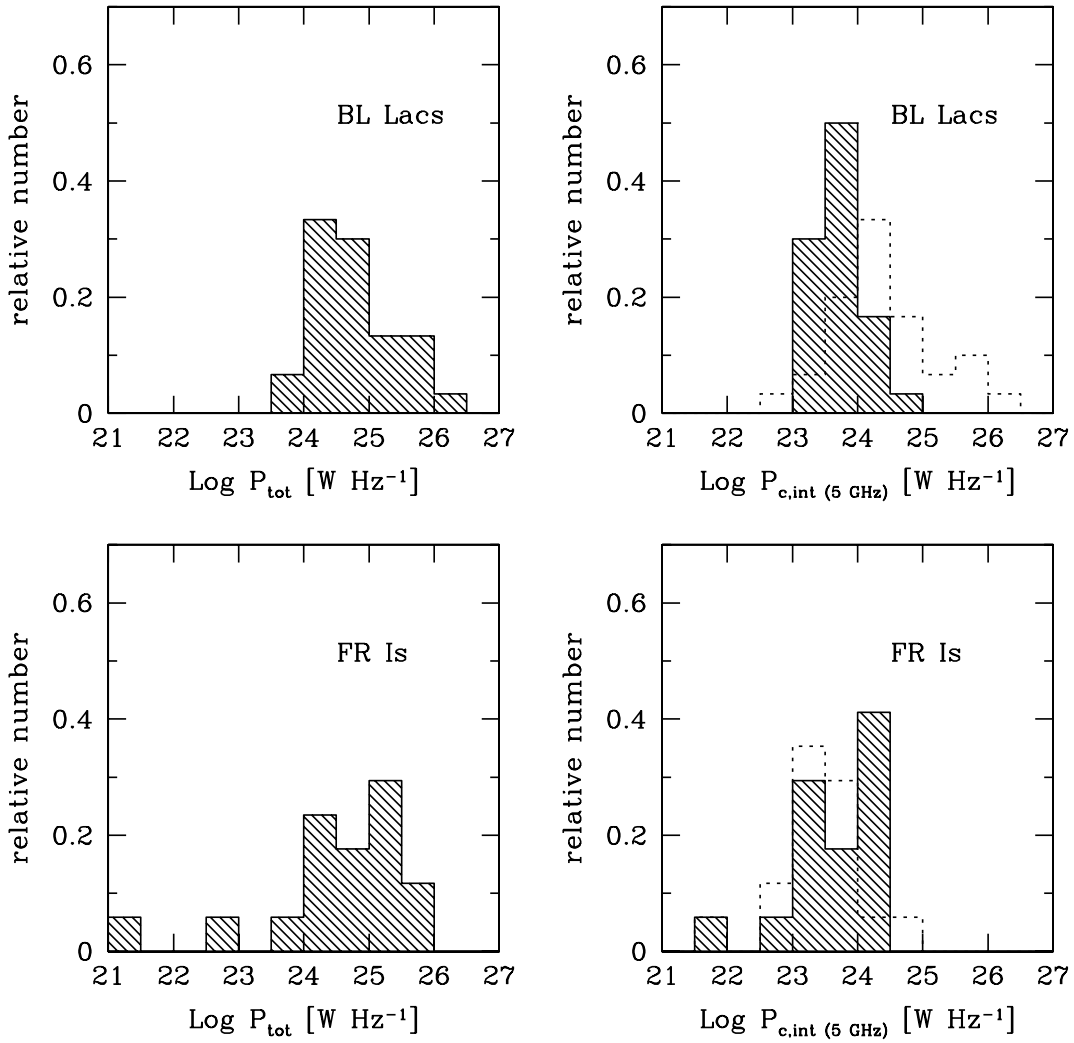

FIG. 12.—Distribution of total and intrinsic core power for objects in the present sample and FR I and low-power compact (LPC) radio galaxies in a sample of radio galaxies (Giovannini et al. 2001). The dashed histograms overlaid on the intrinsic core power show the distribution of the observed values.

properties, being either nonrelativistic or still mildly relativistic in different sources.

It is also interesting to discuss the difference in orientation with respect to more powerful objects by considering the amount of bending in the jets. In particular, large bending is suggestive of small angles, while straight jets are more common in the presence of a larger angle between the jet axis and the line of sight. In Figure 7 we present the bending angle distribution in the 1 Jy sample[5] and for the present sample, excluding those belonging to the 1 Jy sample. The histogram provides a comparison of the two populations, which indicates that high-power BL Lac objects show larger distortions than weak ones. The significance of the difference between the two distributions is quite strong (K-S of 1.42, with a probability that the two distributions are intrinsically similar $\lesssim 0.03$). It is tempting to speculate that this may be ascribed to a different jet orientation, with smaller viewing angles for more powerful and twisting sources. However, it is also possible to give a different interpretation for this occurrence of large bending, if we speculate that FR II galaxies have intrinsically more bent jets than FR I galaxies and that the 1 Jy sample has a parent population in which FR II radio galaxies are a significant fraction. Figure 11 shows the bending angle versus radio power for all the BL Lac objects with available measurements of the bending (from the present work or the 1 Jy sample): there is a weak trend of larger bending in more powerful sources, with a correlation coefficient of $r = 0.42$. In particular, the lack of large bending in low-power sources is remarkable.

While FR II sources may contribute to the parent population of the 1 Jy sample (see also Rector & Stocke 2001), FR I radio galaxies are the best candidates to be the unbeamed counterpart of the objects in the present sample. From our estimate of the jet velocity and orientation, we can derive the intrinsic core radio power: $P_{c,i} = P_{c,o}\delta^{-(2+\alpha)}$. In Figure 12 we present the distribution of the core and low-frequency total radio power for the present sample and the sample of FR I and low-power compact radio galaxies studied by Giovannini et al. (2001). The two samples cover the same range in low-frequency total radio power (Fig. 12, *left*), as expected if FR I galaxies are the parent population of BL Lac objects. We note that the total radio power at 325 MHz should be an intrinsic source property, since the core is self-absorbed and extended lobe emission dominates at low frequency. In the right panels, the shaded

[5] The bending angles for the objects in the 1 Jy sample have been derived by us from maps on parsec and kiloparsec scales published in several works, e.g., Cassaro et al. (1999, 2002), Rector & Stocke (2001), Fomalont et al. (2000), and Shen et al. (1998).

histograms represent the intrinsic core radio power distribution, while the overlaid dashed histograms refer to the observed power of the radio core. Despite a significant difference in the observed values, the distribution of the intrinsic core radio power is similar and in the same range, confirming that the intrinsic properties of the two populations are the same.

We conclude that in our sample the parent population is composed of FR I radio galaxies alone and that the fraction of FR II galaxies in the parent population of BL Lac objects must be very small, if any. FR II galaxies that may be present in the 1 Jy sample must therefore be ascribed to the very large volume considered. In any case, their incidence may be non-negligible among the most powerful LBLs, which could have different properties.

6. CONCLUSIONS

In this paper we have presented a new sample of nearby BL Lac objects with no selection bias on their nuclear radio properties. For sources without good data available in the literature, we present new VLA and VLBA images. Many sources exhibit a resolved radio morphology, as expected if BL Lac objects are FR I radio galaxies oriented at small angles. A few objects show a WAT or head-tail (HT) morphology, suggesting that they are radio galaxies belonging to clusters of galaxies. Most of the arcsecond core flux density is present in our VLBA images; this result implies that we have not missed considerable subarcsecond structure.

On the kiloparsec scale we have both symmetric and one-sided sources, suggesting that kiloparsec-scale jets may have different properties, being either nonrelativistic or still mildly relativistic in different sources. This suggests that the decrease in jet velocity is related to the ISM properties, which can vary among galaxies. More detailed studies with the Expanded Very Large Array (EVLA) or the proposed New Mexico Array are necessary to better investigate this possibility.

Confirming previous results by Rector et al. (2003), parsec- and kiloparsec-scale jets are oriented at the same P.A. in a large fraction of HBLs. Given the relative numbers of HBLs and LBLs in the sample, the low number of distorted structures and the core dominance argument, HBL sources show less distortion and therefore are expected to be oriented at larger angles than the LBL sources. This is confirmed by the core dominance argument, the jet/counterjet ratio, and the synchrotron self-Compton model, under the assumption that all jets possess the same Lorentz factor $\Gamma = 5$. By contrast, if we allow both Γ and θ to vary, we derive similar orientation ($\langle\theta_{\rm LBL}\rangle = 15^\circ \pm 7^\circ$ and $\langle\theta_{\rm HBL}\rangle = 20^\circ \pm 4^\circ$) and a difference in velocity; interestingly, LBLs would have larger bulk velocities (up to $\Gamma \lesssim 7$) than HBLs, including TeV sources ($\langle\Gamma\rangle \sim 3$). In both cases, the Doppler factor of BL Lac objects is considerably smaller in the parsec-scale radio jets than in the γ-ray–emitting region.

In any case, we estimate that most sources ($\sim$80%) in our sample are oriented at an angle to the line of sight larger than 10°. The derived range in orientation corresponds to a possible range of Doppler factors. From these values, we compute the relative intrinsic core radio power and show that intrinsic core radio powers are similar in BL Lac objects and FR I radio galaxies and low-power radio galaxies of the same range of total radio power. No FR II is allowed as the misaligned counterpart of a low-redshift BL Lac object.

We thank the referee, Eric Perlman, for many useful comments and suggestions that improved this work. We also thank D. Dallacasa and A. Treves for critical readings of the paper and valuable suggestions. This research has made use of the NASA/IPAC Extragalactic Database (NED), which is operated by the Jet Propulsion Laboratory, Caltech, under contract with NASA, and of NASA's Astrophysics Data System (ADS) Bibliographic Services. MERLIN is a National Facility operated by the University of Manchester at Jodrell Bank Observatory on behalf of PPARC. This material is based on work supported by the Italian Ministry for University and Research (MIUR) under grant COFIN 2003-02-7534.

REFERENCES

Aharonian, F., et al. 2002, A&A, 384, L23
———. 2003, A&A, 406, L9
Anton, S., Browne, I. W. A., Marcha, M. J. M., Bondi, M., & Polatidis, A. 2004, MNRAS, in press, doi: 10.1111/j.1365-2966.2004.07961.x
Antonucci, R. R. J., & Ulvestad, J. S. 1985, ApJ, 294, 158
Appl, S., Sol, H., & Vicente, L. 1996, A&A, 310, 419
Attridge, J. M., Roberts, D. H., & Wardle, J. F. C. 1999, ApJ, 518, L87
Baum, S. A., et al. 1997, ApJ, 483, 178
Becker, R. H., White, R. L., & Helfand, D. J. 1995, ApJ, 450, 559
Biretta, J. A., Sparks, W. B., & Macchetto, F. 1999, ApJ, 520, 621
Caccianiga, A., & Marchã, M. J. M. 2004, MNRAS, 348, 937
Cassaro, P., Stanghellini, C., Bondi, M., Dallacasa, D., della Ceca, R., & Zappalà, R. A. 1999, A&AS, 139, 601
Cassaro, P., Stanghellini, C., Dallacasa, D., Bondi, M., & Zappalà, R. A. 2002, A&A, 381, 378
Catanese, M., et al. 1998, ApJ, 501, 616
Celotti, A., Maraschi, L., Ghisellini, G., Caccianiga, A., & Maccacaro, T. 1993, ApJ, 416, 118
Chiaberge, M., Celotti, A., Capetti, A., & Ghisellini, G. 2000, A&A, 358, 104
Condon, J. J., Cotton, W. D., Greisen, E. W., Yin, Q. F., Perley, R. A., Taylor, G. B., & Broderick, J. J. 1998, AJ, 115, 1693
Costamante, L., & Ghisellini, G. 2002, A&A, 384, 56
Danziger, I. J., Fosbury, R. A. E., Goss, W. M., & Ekers, R. D. 1979, MNRAS, 188, 415
Donato, D., Ghisellini, G., Tagliaferri, G., & Fossati, G. 2001, A&A, 375, 739
Donato, D., Gliozzi, M., Sambruna, R. M., & Pesce, J. E. 2003, A&A, 407, 503
Douglas, J. N., Bash, F. N., Bozyan, F. A., Torrence, G. W., & Wolfe, C. 1996, AJ, 111, 1945
Falomo, R. 1994, Messenger, 77, 49
Falomo, R., Kotilainen, J. K., & Treves, A. 2002, ApJ, 569, L35
Falomo, R., Pesce, J. E., & Treves, A. 1995, ApJ, 438, L9
Falomo, R., Scarpa, R., & Bersanelli, M. 1994, ApJS, 93, 125
Falomo, R., Scarpa, R., Treves, A., & Urry, C. M. 2000, ApJ, 542, 731
Feretti, L., Perley, R., Giovannini, G., & Andernach, H. 1999, A&A, 341, 29
Fey, A. L., & Charlot, P. 2000, ApJS, 128, 17
Fomalont, E. B., Frey, S., Paragi, Z., Gurvits, L. I., Scott, W. K., Taylor, A. R., Edwards, P. G., & Hirabayashi, H. 2000, ApJS, 131, 95
Fossati, G., Maraschi, L., Celotti, A., Comastri, A., & Ghisellini, G. 1998, MNRAS, 299, 433
Gabuzda, D. C., & Cawthorne, T. V. 2003, MNRAS, 338, 312
Ghisellini, G., Celotti, A., Fossati, G., Maraschi, L., & Comastri, A. 1998, MNRAS, 301, 451
Ghisellini, G., Padovani, P., Celotti, A., & Maraschi, L. 1993, ApJ, 407, 65
Giovannini, G. 2003, NewA Rev., 47, 551
Giovannini, G., Cotton, W. D., Feretti, L., Lara, L., & Venturi, T. 2001, ApJ, 552, 508
Giovannini, G., Falomo, R., Scarpa, R., Treves, A., & Urry, C. M. 2004, ApJ, 613, 747
Giovannini, G., Feretti, L., Gregorini, L., & Parma, P. 1988, A&A, 199, 73
Giovannini, G., Feretti, L., Venturi, T., Lara, L., Marcaide, J., Rioja, M., Spangler, S. R., & Wehrle, A. E. 1994, ApJ, 435, 116
Giroletti, M., et al. 2004, ApJ, 600, 127
Gómez, J., & Marscher, A. P. 2000, ApJ, 530, 245
Green, R. F., Schmidt, M., & Liebert, J. 1986, ApJS, 61, 305
Hanasz, M., & Sol, H. 1996, A&A, 315, 355
Holder, J., et al. 2003, ApJ, 583, L9

Homan, D. C., Ojha, R., Wardle, J. F. C., Roberts, D. H., Aller, M. F., Aller, H. D., & Hughes, P. A. 2001, ApJ, 549, 840
Horan, D., et al. 2002, ApJ, 571, 753
Jannuzi, B. T., Smith, P. S., & Elston, R. 1994, ApJ, 428, 130
Jorstad, S. G., Marscher, A. P., Mattox, J. R., Wehrle, A. E., Bloom, S. D., & Yurchenko, A. V. 2001, ApJS, 134, 181
Keel, W. C. 1986, ApJ, 302, 296
Kollgaard, R. I., Gabuzda, D. C., & Feigelson, E. D. 1996, ApJ, 460, 174
Laing, R. A., & Bridle, A. H. 2002, MNRAS, 336, 1161
Landt, H., Padovani, P., Perlman, E. S., Giommi, P., Bignall, H., & Tzioumis, A. 2001, MNRAS, 323, 757
Lara, L., Giovannini, G., Cotton, W. D., Feretti, L., & Venturi, T. 2004, A&A, 415, 905
Laurent-Muehleisen, S. A., Kollgaard, R. I., Moellenbrock, G. A., & Feigelson, E. D. 1993, AJ, 106, 875
Lin, Y. C., et al. 1995, ApJ, 442, 96
Lister, M. L., Marscher, A. P., & Gear, W. K. 1998, ApJ, 504, 702
Marscher, A. P. 1987, in Superluminal Radio Sources, ed. J. A. Zensus & T. J. Pearson (Cambridge: Cambridge Univ. Press), 280
Meier, D. L. 2003, NewA Rev., 47, 667
Morganti, R., Killeen, N. E. B., & Tadhunter, C. N. 1993, MNRAS, 263, 1023
Morris, S. L., Stocke, J. T., Gioia, I. M., Schild, R. E., Wolter, A., Maccacaro, T., & della Ceca, R. 1991, ApJ, 380, 49
Murphy, D. W., Browne, I. W. A., & Perley, R. A. 1993, MNRAS, 264, 298
Nishiyama, T., et al. 1999, Proc. 26th Int. Cosmic-Ray Conf. (Salt Lake City), 370
O'Dea, C. P., Barvainis, R., & Challis, P. M. 1988, AJ, 96, 435
Orr, M. J. L., & Browne, I. W. A. 1982, MNRAS, 200, 1067
Padovani, P., & Giommi, P. 1995, MNRAS, 277, 1477
Padovani, P., Perlman, E. S., Landt, H., Giommi, P., & Perri, M. 2003, ApJ, 588, 128
Perlman, E. S. 1994, Ph.D. thesis, Univ. Colorado
Perlman, E. S., Biretta, J. A., Sparks, W. B., Macchetto, F. D., & Leahy, J. P. 2001, ApJ, 551, 206
Perlman, E. S., Biretta, J. A., Zhou, F., Sparks, W. B., & Macchetto, F. D. 1999, AJ, 117, 2185
Perlman, E. S., Padovani, P., Giommi, P., Sambruna, R., Jones, L. R., Tzioumis, A., & Reynolds, J. 1998, AJ, 115, 1253
Perlman, E. S., & Stocke, J. T. 1993, ApJ, 406, 430
Perlman, E. S., et al. 1996, ApJS, 104, 251
Pesce, J. E., Sambruna, R. M., Tavecchio, F., Maraschi, L., Cheung, C. C., Urry, C. M., & Scarpa, R. 2001, ApJ, 556, L79
Pian, E., Falomo, R., Ghisellini, G., Maraschi, L., Sambruna, R. M., Scarpa, R., & Treves, A. 1996, ApJ, 459, 169
Piccinotti, G., Mushotzky, R. F., Boldt, E. A., Holt, S. S., Marshall, F. E., Serlemitsos, P. J., & Shafer, R. A. 1982, ApJ, 253, 485
Piner, B. G., & Edwards, P. G. 2004, ApJ, 600, 115
Rector, T. A., Gabuzda, D. C., & Stocke, J. T. 2003, AJ, 125, 1060
Rector, T. A., & Stocke, J. T. 2001, AJ, 122, 565
Rector, T. A., Stocke, J. T., Perlman, E. S., Morris, S. L., & Gioia, I. M. 2000, AJ, 120, 1626
Reid, R. I., Kronberg, P. P., & Perley, R. A. 1999, ApJS, 124, 285
Rengelink, R. B., Tang, Y., de Bruyn, A. G., Miley, G. K., Bremer, M. N., Roettgering, H. J. A., & Bremer, M. A. R. 1997, A&AS, 124, 259
Sambruna, R. M., Maraschi, L., & Urry, C. M. 1996, ApJ, 463, 444
Scarpa, R., Falomo, R., & Pian, E. 1995, A&A, 303, 730
Scarpa, R., Urry, C. M., Falomo, R., Pesce, J. E., & Treves, A. 2000, ApJ, 532, 740
Scarpa, R., Urry, C. M., Falomo, R., & Treves, A. 1999, ApJ, 526, 643
Schachter, J. F., et al. 1993, ApJ, 412, 541
Schwab, F. R., & Cotton, W. D. 1983, AJ, 88, 688
Shen, Z.-Q., et al. 1998, AJ, 115, 1357
Shepherd, M. C., Pearson, T. J., & Taylor, G. B. 1994, BAAS, 26, 987
———. 1995, BAAS, 27, 903
Slinglend, K., Batuski, D., Miller, C., Haase, S., Michaud, K., & Hill, J. M. 1998, ApJS, 115, 1
Sol, H., Pelletier, G., & Asseo, E. 1989, MNRAS, 237, 411
Sparks, W. B., Biretta, J. A., & Macchetto, F. 1994, ApJS, 90, 909
Stickel, M., Fried, J. W., Kuehr, H., Padovani, P., & Urry, C. M. 1991, ApJ, 374, 431
Stickel, M., & Kuehr, H. 1994, A&AS, 103, 349
Stocke, J. T., Morris, S. L., Gioia, I. M., Maccacaro, T., Schild, R., Wolter, A., Fleming, T. A., & Henry, J. P. 1991, ApJS, 76, 813
Tavecchio, F., Maraschi, L., & Ghisellini, G. 1998, ApJ, 509, 608
Tingay, S. J., & Edwards, P. G. 2002, AJ, 124, 652
Urry, C. M., & Padovani, P. 1995, PASP, 107, 803
Urry, C. M., Scarpa, R., O'Dowd, M., Falomo, R., Pesce, J. E., & Treves, A. 2000, ApJ, 532, 816
Veron-Cetty, M.-P., & Veron, P. 1993, A&AS, 100, 521
Wardle, J. F. C., Moore, R. L., & Angel, J. R. P. 1984, ApJ, 279, 93
Wrobel, J. M., & Lind, K. R. 1990, ApJ, 348, 135